Mathematical modeling suggests that a single Plasmodium-specific CD8 T cell can eliminate a malaria liver stage in mice

Soumen Bera[1*], Rogerio Amino[2], Ian A. Cockburn[3], and Vitaly V. Ganusov[1,4*]

[1] *Department of Microbiology, University of Tennessee, Knoxville, TN 37996, USA*
[2] *Unit of Malaria Infection and Immunity, Institut Pasteur, 75015, Paris, France*
[3] *Division of Immunology, Inflammation and Infectious Disease, John Curtin School of Medical Research, The Australian National University, Canberra, 2600, Australia*
[4] *Department of Mathematics, University of Tennessee, Knoxville, TN 37996, USA*
[*] *Corresponding authors: soumenmath4189@gmail.com, vitaly.ganusov@gmail.com*

May 18, 2022

Abstract

Vaccination strategies in mice inducing high numbers of memory CD8 T cells specific to a single epitope are able to provide sterilizing protection against infection with Plasmodium sporozoites. We have recently suggested that formation of clusters of activated/memory CD8 T cells around Plasmodium-infected hepatocytes is important in providing such protection. While we have shown that formation of such clusters is relatively rapid, many questions of how clustered CD8 T cells eliminate the infection remain unanswered. Specifically, we still do not know if one T cell can kill the parasite, how long it takes for T cells to eliminate the infection, and whether individual T cells in the cluster cooperate or compete in killing the parasite. To address these questions, we used our previously generated data in which we employed intravital microscopy to longitudinally image 32 GFP-expressing Plasmodium yoelii parasites in livers of mice that had received activated Plasmodium-specific CD8 T cells after sporozoite infection. We found great heterogeneity in the dynamics of the normalized GFP signal from the parasites (termed "vitality index" or VI) that was weakly correlated with the number of T cells near the parasite. We found that a simple model assuming mass-action killing by independent T cells relatively well describes the decay of VI over time for a subset of parasites (8/32). Given the estimated average per capita kill rate of $k = 0.049$/h even a single T cell should be able to kill the parasite in 48 hour lifespan of the liver stage. Stochastic simulations suggested that the observed constant VI in the majority of parasites cannot be explained with the estimated kill rate and the observed numbers of T cells in clusters suggesting that for such parasites either T cells do not recognize the infection or the parasite actively resists killing. Taken together, our analysis provides novel insights into how CD8 T cells control individual intracellular infections in vivo.

Keywords: CD8+ T cell, Plasmodium parasite, liver stages, intravital imaging, mathematical modeling

Abbreviations: Py - Plasmodium yoelii, GFP - green fluorescent protein, VI - vitality index, DDR - density-dependent recruitment.

1 Introduction

Malaria is a mosquito-born disease caused by parasites from genus Plasmodium; the Plasmodium parasites of humans are responsible for more than 200 million infections and 500,000 death annually [1]. Infection starts when mosquitoes inject sporozoites (a specific stage of Plasmodium parasites) into dermal tissue [2]. The sporozoites move in the tissue, find blood vessels, invade into the blood vessels, and disseminate in the body with the blood. Some sporozoites invade the liver, infect hepatocytes and form liver stages. It takes approximately 2 days (in mice) or 6-7 days (in humans) for liver stages to develop into merozoites (another stage of malaria parasites) [3]. Merozoites infect red blood cells and ultimately cause clinical symptoms of malaria. Several vaccine candidates aim at preventing the disease; some of these aim at removing all liver stages by inducing large numbers of Plasmodium-specific memory CD8 T cells [4–6].

Multiple strategies have been used to generate large numbers of Plasmodium-specific CD8 T cells including priming mice with dendritic cells (DCs) coated with Plasmodium peptides and boosting with Listeria monocytogenes (LM), expressing Plasmodium peptides, immunization with radiation-attenuated sporozoites (RAS), and adoptive transfer of in vitro activated CD8 T cells [4, 7–12]. While these strategies have shown good protection following exposure to Plasmodium sporozoites (e.g., [4, 13]), specific mechanisms by which vaccine-induced CD8 T cells find the inflected cells and critical parameters required for parasite's killing such as the number and duration of CD8 T cell contacts with parasitized cells, remain largely unknown.

Intravital microscopy has been used to gain quantitative insights into the process by which CD8 T cells kill their targets in vivo. In particular, as far as we are aware, Mempel *et al.* [14] were the first to directly observe killing of targets (peptide-pulsed B cells) by CD8 T cells in vivo. Interestingly, the authors found that formation of the conjugate between the T cell and its target eventually resulted in arrest of the target cell movement and indication of the target cell death within 20-30 min after initial contact [14]. In contrast, killing of cancer cells by adoptively transferred activated CD8 T cells on average took 6 hours [15]. As far as we are aware we were the first to document kinetics of killing of individual parasitized cells by CD8 T cells in vivo [16]. In that study by using intravital microscopy we followed the kinetics of formation of clusters of Plasmodium-specific CD8 T cells around Plasmodium liver stages in murine livers; interestingly, a formation of larger clusters (3 or more cells present within 40 μm of the parasite) was associated with a higher chance of parasite's death during the imaging period [16]. Also, based on the kinetics of the loss of fluorescence signal from the GFP-expressing parasites we observed four different patterns of parasite's death but the actual killing kinetics was not quantified [16]. Recent work extended our observations to CD8 T cell-mediated killing of virus-infected cells suggesting that after initial contact, it takes on average 30 minutes for the T cell to kill its target [17]. Interestingly, while the initial analysis suggested that there may be cooperation between individual CD8 T cells bound to the same virus-infected cells, further analysis suggested that such a conclusion may be an artifact of the data analysis that ignored prolonged "zombie" contacts of CD8 T cells with already dying targets [17, 18]. Another study suggested that killing of cancer cells may require several contacts by the same or different CD8 T cells occurring within a short (< 1 h) time period [19].

Following our previous work here we provide comprehensive quantitative analysis of the data on the kinetics of CD8 T cell-mediated killing of Plasmodium liver stages. In these experiments we could accurately monitor the number of Plasmodium-specific CD8 T cells located in the vicinity of GFP-expressing liver stages and "health" of the liver stages (indicated by the relative magnitude of

the GFP signal) for several hours for 32 individual parasites [16]. Most of the liver stages (26/32) had at least a single CD8 T cells nearby at some point of imaging, and our recently developed density-dependent recruitment model of T cell cluster formation could reasonably well describe the kinetics of accumulation of Plasmodium-specific CD8 T cells near individual parasites over time. Interestingly, the decline of the relative GFP signal (named "vitality index" or VI) was observed only for a subset of parasites (8/26), and fitting a simple mathematical model to the VI decline allowed to estimate the per capita killing efficiency of Plasmodium-specific CD8 T cells in vivo. We did not find any evidence that CD8 T cells cooperate in parasite's killing as the basic, mass action-based model could describe the data well. Stochastic simulations of formation of CD8 T cell clusters around Plasmodium-liver stages and their killing suggested that the duration of the experiments should be sufficient to detect impact of T cells on the VI dynamics — this, however, contradicts observations in which many liver stages had stable VI. These results strongly suggest that either for such parasites despite being in the proximity of infection CD8 T cells are not able to recognize the parasite or that such parasites actively resist killing.

2 Materials and methods

2.1 Experimental Data

Experimental data for our analyses have been generated in our previously published work [16] except the novel data on the dynamics of the vitality index (VI, see below) in control mice. In short, there were two sets of experiments performed (**Figure 1**A). In control experiments, Balb/c mice were infected with 3×10^5 GFP-expressing Plasmodium yoelii (Py) sporozoites i.v., and 24h later the livers of mice were surgically exposed and imaged using a spinning disk confocal microscope. In total, 38 parasites in 2 different mice were followed for 6 hours. Imaging data from 22 of such parasites were analyzed longitudinally. Specifically, the vitality index (VI) of each parasite at different times was calculated in ImageJ as the $\log_{10}$ of the parasite brightness to the background brightness in the GFP channel using maximal z projection. In control experiments parasites were defined as superficial or deep based on their higher or lower z position in the stack of images, respectively (e.g., **Supplemental Figure S1**).

In treatment experiments, mice were infected with 3×10^5 GFP-expressing Py sporozoites. Twenty hours later, 9×10^6 activated Py-specific CD8 T cells were transferred into infected mice (details of how activated Py-specific CD8 T cells were generated, see [16]). Four to eight hours later, livers of mice were surgically exposed and imaged using a spinning disk confocal microscope. In total, 32 parasites were followed in 4 mice. VI was calculated for each parasite, and by segmenting the movies with Imaris, the number of T cells found within 40 μm of the liver stage over time was quantified [20–22]. Following previous analysis we assume that the parasite is considered dead if the VI becomes less than 0.2 [16]. Our main results, however, were not particularly sensitive to this assumption (see Results section).

We provide all numeric experimental data as the supplement to the paper. These data include the following.

(a) For control experiments, imaging was performed from 24 hour to 30 hour and from 30 hour to 33 hour after infection in 2 mice, respectively. The data include VI over time for each parasite

(**Figure 1**Bi and **Supplemental Figure S1**A).

(b) For treatment experiments, imaging was performed in different intervals that typically varied per mouse but also per parasite: 4 to 6.2 hours, 8 to 11.8 hours, 5 to 9.12 hours, 6 to 9.12 hours, 6.5 to 7.32 hours, and 7.82 to 11 hours in four different mice (**Figure 1**Bii-Biii and **Supplemental Figure S1**B-D). For every mouse and parasite ID, the data include the time since infection (hours), the number of T cells per parasite, GFP of the background and the parasite, and the parasite's VI.

In cases when VI or T cell number per parasite could not be calculated (due to imaging artifacts), values were indicated as NA. These data were excluded in the analysis.

2.2 Mathematical models

2.2.1 Dose response models to predict parasite's VI from T cell numbers

In our data both parasite's VI and T cell numbers per parasite change over time. In addition to modeling the dynamics of VI change (see below) we aggregated the data and calculated the relationship between the VI and T cell numbers per parasite at a given time point t. For the analysis we normalized the VI for each parasite to its initial value found at the beginning of imaging. To describe the "dose" relationship between the VI and the number of CD8 T cells we used several alternative models. These include log-logistics model:

$$V(T(t), \beta_1, \beta_2, \beta_3, \beta_4) = \beta_2 + \frac{\beta_3 - \beta_2}{1 + \mathrm{e}^{\beta_1(\log(T(t)-\log(\beta_4)))}}, \tag{1}$$

where β_1 denoting the steepness of the dose-response curve, β_2, β_3 the lower and upper limit of the response and β_4 represent the effective dose ED50. Other models are

$$\begin{aligned}
V(T(t), \bar{\beta}) &= \beta_2 + (\beta_3 - \beta_2)\mathrm{e}^{-\mathrm{e}^{\beta_1(\log(T(t)-\log(\beta_4))}}, && (2)\\
V(T(t), \bar{\beta}) &= \beta_2 + (\beta_3 - \beta_2)(1 - \mathrm{e}^{-\mathrm{e}^{\beta_1(\log(T(t)-\log(\beta_4))}}), && (3)\\
V(T(t), \bar{\beta}) &= \beta_2 + (\beta_3 - \beta_2)N(\ln(T(t)) - \ln(\beta_4), \beta_1), && (4)\\
V(T(t), \bar{\beta}) &= \beta_2 + (\beta_3 - \beta_2)\mathrm{e}^{-\frac{T(t)}{\beta_4}}, && (5)
\end{aligned}$$

where eqns. (2)–(5) are for Weibull I, Weibull II, log-normal, and exponential functional response, respectively; N is normal distribution function. We fitted these models to data using R package *drc*. In *drc*, parameters are estimated using maximum likelihood that is under the assumption of normally distributed response simplifies to nonlinear least squares [23]. From the parameter estimates we calculated T_{IC50} as number of CD8 T cells required for 50% inhibition of parasite's VI from its initial value. Typically, T_{IC50} was computed numerically by setting $V = 0.5$ in the model and solving for $T(t)$ with estimated parameters $\bar{\beta}$.

2.2.2 Mixed effect modeling of VI dynamics

To separate the effect of time (t), T cell number per parasite (T), and mouse effect (M) in the VI dynamics we performed linear mixed-effect modeling analysis. Using *lme4* package in R we considered the following alternative models that take into account time since T cell transfer t and the number of T cells per parasite T:

$$
\begin{aligned}
V &\sim t, && (6)\\
V &\sim t + 1|T, && (7)\\
V &\sim t \times T + 1|T, && (8)\\
V &\sim t + 1|T + 1|t : T. && (9)
\end{aligned}
$$

To determine potential impact of individual mice on the VI dynamics we considered the following models:

$$
\begin{aligned}
V &\sim t + 1|M + 1|T, && (10)\\
V &\sim t + 1|M + 1|M/T, && (11)\\
V &\sim t \times T + 1|M/T, && (12)\\
V &\sim t + 1|M/T + 1|t : T, && (13)
\end{aligned}
$$

where notations are defined as follows: $1|T$ is represent a random effect upon VI after a fixed effect, $1|M$ is defined a random effect of four different mice upon VI, $t \times T$ is defined main effect with interaction between time and T cells, $1|M/T$ indicates a nested random effect of T cells from different mice, $1|t : T$ is used to define a random effect with interaction between T cell number and time. This analysis was performed on 26 parasites that had at least one T cell nearby during imaging. All models were compared with the null model (no T cells or mouse effect) using ANOVA, and the best model was determined based on the lowest Akaike Information Criterion (AIC) value [24, 25].

2.2.3 A forecasting statistical model to estimate next VI from previous VI and T cell numbers

To investigate whether CD8 T cells may impact dynamics of parasite's VI in subtle ways we borrowed a forecasting approach from economics and several alternative mathematical models from disease population ecology [26]. The basic idea of the model is to use information on the parasite's VI (V_t) and T cell number around the parasite (T_t) at time t to predict parasite's VI at time $t + 1$. We consider the following alternative models:

$$
\begin{aligned}
V_{t+1} &= (1 + r)V_t, && (14)\\
V_{t+1} &= (1 + r)V_t - kV_t^{\alpha}T_t^{\beta}, && (15)
\end{aligned}
$$

where r is the growth rate of the VI and k is the killing rate of the VI by T cells in eqns. (14)–(15). Departures from the mass-action killing of the parasite by T cells are modelled with parameter β with $\beta > 1$ indicating cooperation at killing and $\beta < 1$ indicating competition at killing.

We fitted these model to the parasite's VI using linear regression (least squares) by taking V_t and T_t given in the data and predicting V_{t+1} also found in the data. Specifically, for V_{t+1} we took observed values for VI for a given parasite starting at time point $t = 2$ and regressed this vector against VI values starting at $t = 1$ until $t = N - 1$ where N is the number of data points for each specific parasite. To investigate if different dynamics of T cell numbers per parasite may allow for a better description of VI dynamics we allowed the number of T cells per parasite i) to change randomly, ii) to increase over time from the lowest number found in the data for a given parasite to 10 (maximal value in our data), and iii) to decrease over time from the highest number of T cells found in the data for a given parasite to zero (lowest value found in our data).

2.2.4 Mechanistic modeling of T cell clustering dynamics

To describe the net change in the average number of T cells around a given parasite over time ($T(t)$) we use a density-dependent recruitment (DDR) model that as we showed previously described clustering of CD8 T cells with best quality [16, 22]:

$$T(t) = \frac{\lambda_0}{\mu - \lambda_1}(1 - e^{-(\mu-\lambda_1)t}), \tag{16}$$

where λ_0 and λ_1 are the initial T cell recruitment into the cluster and the amplification rate of the T cell cluster formation, respectively, μ is the per capita exit rate of T cells from the cluster, and the initial condition is $T(0) = 0$ [22]. It should be noted that to describe typical cluster dynamics data with finite cluster size $\mu > \lambda_1$ and that only the difference $\mu - \lambda_1$ can be estimated from the average cluster data. We have shown recently by analyzing clustering of T cells longitudinally that parameters of this model are likely to be time-dependent and are expected to decline with time since infection [22]. Since we only use the average number of T cells per parasite, specific details of how T cell numbers reach relatively constant numbers are not crucial for our analyses. To estimate model parameters (λ_0 and $\mu - \lambda_1$) we fitted eqn. (16) to the experimentally measured number of T cells per parasite over time for each parasite using least squares in function nlsLM in R (using package minpack.lm) with control maxfev=10000 with maxiter=1024 [27].

2.2.5 Mechanistic modeling of VI dynamics

To further understand whether CD8 T cells compete or cooperate in killing of the parasite and to estimate the per capita killing efficiency of Plasmodium-specific CD8 T cells we used the following models for the dynamics of parasite's VI

$$\frac{\mathrm{d}V_t}{\mathrm{d}t} = rV_t - kV_tT(t), \tag{17}$$

$$\frac{\mathrm{d}V_t}{\mathrm{d}t} = rV_t - kV_tT(t)^n, \tag{18}$$

$$\frac{\mathrm{d}V_t}{\mathrm{d}t} = rV_t - kV_t\frac{T(t)^n}{h^n + T(t)^n}, \tag{19}$$

where V_t represents the parasites VI at time t (in hours), r is the rate of VI's growth, k is the killing efficiency of CD8 T cells, h is half-saturation constant and n is Hill coefficient, indicating deviation of the killing from mass-action (in eqn. (18)). The dynamics of the number of CD8 T cells per parasite $T(t)$ is given in eqn. (16). The models were fitted to the dynamics of VI in a subset of parasites for which VI was negatively correlated with the number of T cells per parasite (8 parasites). The initial value for VI was estimated from the data. The models were fitted using least squares using the Levenberg-Marquardt method from *scipy.optimize.leastsq* in Python. We estimated the standard error for model parameters from the estimated covariance matrix. For each model (three different functional responses) we performed the above procedure separately for each of 8 parasites. We then used the AIC to select the best model from the three different functional CD8 T cell responses:

$$AIC = N \ln\left[\frac{SSR}{N}\right] + 2N_p, \tag{20}$$

where SSR is the sum of squared residuals from the fit, N is the number of data points and N_p is the number of model parameters fitted to data [24, 25].

2.2.6 Fitting a mechanistic model of T cell-mediated killing using Bayesian approach

To more accurately estimate the efficiency at which Plasmodium-specific CD8 T cells reduce parasite's VI we fitted the simplest model (eqn. (17)) to the dynamics of VI for 8 parasites (see above) using Bayesian approach. To fit the model we used package PyMC3 [28] in python. We have applied 'no u-tern' sampling to produce 10,000 posterior samples from 2 independent MCMC chains that parameterized the following model:

$$\log(V) \sim \mathcal{N}(\log V0 - kT(t),\, \sigma^2), \tag{21}$$

where $\mathcal{N}(\mu, \sigma^2)$ denotes normal distribution with mean μ and variance σ^2. We used the following uninformative prior distributions for the model parameters:

$$k \sim \mathcal{N}(\mu = 0, \sigma = 100), \tag{22}$$

$$\sigma(x) \sim \frac{2\pi\beta}{(1+x^2)(\pi\beta + 2(1-\beta)\tan^{-1} x)^2}, \tag{23}$$

where $\beta = 2$ for half Cauchy distribution (eqn. (23)). Note that our posterior assumption did not appear to depend on this choice; for example, we found the same results with an inverse gamma prior.

2.2.7 Stochastic model of variability of parasite's VI over time

To investigate VI variability that many come from stochasticity of parasite's dynamics we performed stochastic simulations of the parasite's VI in the presence of different numbers of T cells near the parasite using Gillespie's algorithm [29]. Simulations were performed to mimic experimental design. Specifically, in experiments GFP signal from the parasite could theoretically vary between 0-255 in unit increments (8 bit), and typically, by the start of imaging, GFP signal rarely exceeded 200 with background being 10-20. For simplicity we assume that parasite's health signal starts at 100 with the background being 1, resulting in the initial VI being $\log_{10}(100/1) = 2$. Parasite's GFP signal was allowed to grow over time with a minimal growth rate ($r = 0.0001/\text{h}$) for twenty hours while background remained fixed. At this time, T cells were transferred into mice; T cells accumulated at the parasite at the rate defined by parameters λ_0 and $\mu - \lambda_1$ (see eqn. (16)) and killed the parasite at a rate k. The simulations were run for another 36 hours. Two hundred simulations were run using python package *gillespy2* with *Tau-Hybrid* solver. In another set of simulations instead of modeling increase in T cell numbers near the parasite we allowed T cell numbers to change randomly over time in the range observed for a given parasite.

3 Results

3.1 Experimental framework to quantify how *Plasmodium*-specific CD8 T cells kill *Plasmodium yoelii* parasites in the liver

To understand how Plasmodium-specific CD8 T cells may eliminate Plasmodium yoelii (Py) sporozoite from the liver we have performed intravital imaging experiments in which GFP-expressing parasites were imaged in the livers of live mice using intravital microscopy [16, **Figure 1**A]. From these imaging data, we calculated the relative brightness of the GFP signal from Py liver stages (denoted as vitality index or VI) in both control and treatment experiments (**Figure 1**Bi-Bii) and the number of Plasmodium-specific CD8 T cells located within a short distance from the parasite at different times after T cell transfer in treatment experiments (**Figure 1**Biii).

In control experiments in which no T cells were transferred, VI remained constant for all except of one parasite that were followed longitudinally (**Supplemental Figure S1**A). Estimated growth rates of the VI on average did not significantly differ from 0 ($p = 0.92$ and $p = 0.13$ for mouse 1 and 2, respectively, Sign-Ranked test) suggesting that in the absence of T cells, the VI does not increase over several hours of the imaging experiments. This is perhaps expected given that the VI denotes the relative GFP intensity and true parasite's growth may be better estimated by the size of the liver stage [30]. Interestingly, the actual value of the VI varied for different parasites with the parasites in deeper tissues (as judged by the slice's z coordinate) but most were above of VI = 0.2 which was previously defined as a VI cutoff for a dead/dying parasite [16].

Importantly, VI was more variable over time and between individual parasites in mice that had received Py-specific T cells (**Figure 1**Bii, **Supplemental Figure S1**B, **Supplemental Figure S2** and **Supplemental Figure S3**). In these experiments only 6 out of 32 of the liver stages were not surveyed by T cells over the imaging period (i.e., no T cells were within 40 μm of the parasite, **Supplemental Figure S1**C and **Supplemental Figure S4**); the change in the number of T cells in the vicinity of each parasite was variable with some parasites accumulating more T cells while

others loosing T cells, and some parasites being surveyed by a single T cell at some time point (**Figure 1**Biii and **Supplemental Figure S4**). Interestingly, many parasites had stable VI despite having multiple T cells nearby (e.g., **Supplemental Figure S3**) and only a relatively small subset of parasites had a statistically significant decline in the VI over imaging time period.

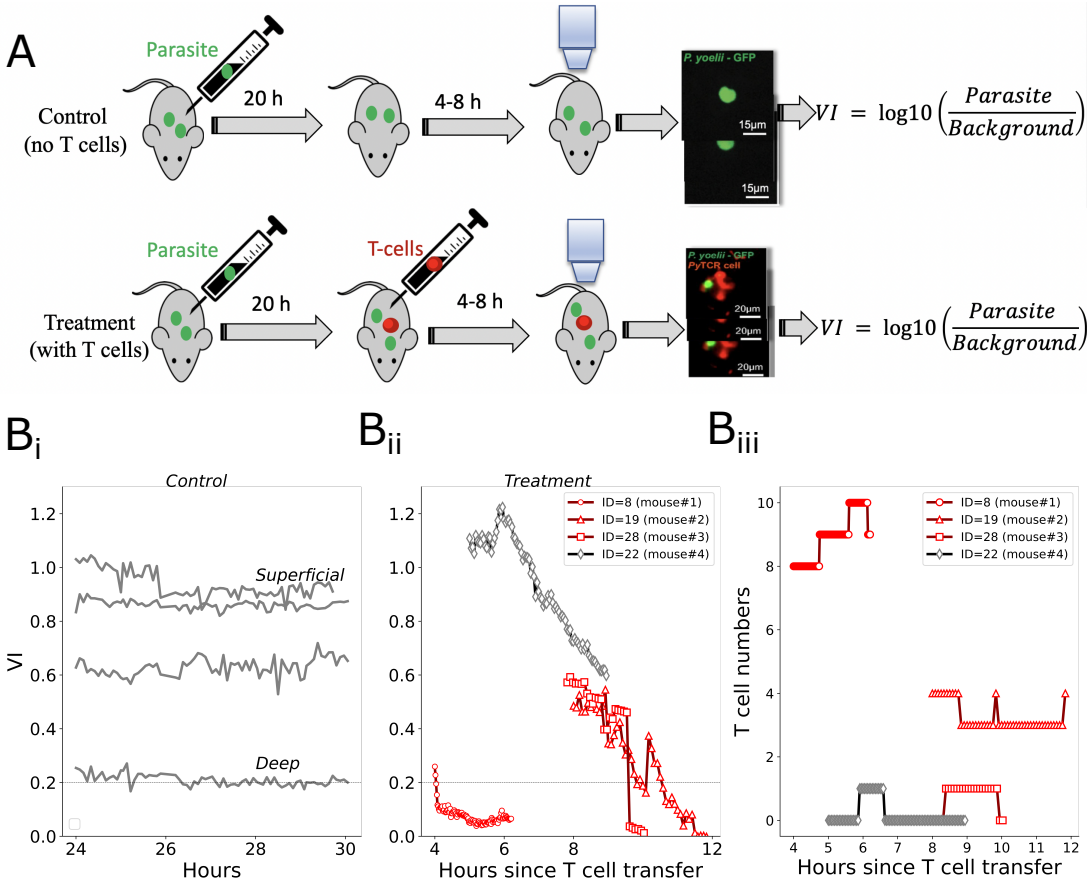

Figure 1: Experimental design to measure T cell impact on Plasmodium liver stages. **(A)** Experimental design. Mice were infected with 3×10^5 GFP-expressing Py sporozoites and divided into two groups as control or treatment. In the control group mice were left until imaging started 24-28 hours after the infection. In the treatment group, 9×10^6 Py-specific activated CD8+ T cells (PyTCR) were transferred into infected mice 20 hours after infection. Four to eight hours later, murine livers were surgically exposed and z-stacks of images were taken using spinning disk confocal microscope [16]. Vitality index (VI) of a given parasite was calculated as the $\log_{10}$ of the ratio between brightness of the GFP signal from the parasite to the brightness of the background based on maximal z projections. The number of T cells within 40 μm of each liver stage was also calculated. **(Bi,Bii)**: Example of the VI dynamics for control (Bi) or treatment (Bii) groups. "Superficial" and "deep" denote location of the parasite based on the z coordinate in the imaging data. **(Biii)** Change in the number of Py-specific CD8+ T cells near the Py-infected hepatocytes over time since T cell transfer. See **Supplemental Figure S1** for all data graphs.

3.2 The number of T cells per parasite negatively correlates with parasite's VI

To better understand how the number of CD8 T cells per parasite is related to the parasite's VI and how imaging of individual mice may influence the results, we performed several alternative analyses. First, we analyzed the relationship between the VI and the number of T cells per parasite for each mouse. Interestingly, we found that a higher number of T cells per parasite was negatively correlated with the parasite's VI for three out of four mice (**Figure 2**A). There was no correlation between

CD8 T cell numbers per parasite and parasite's VI for most parasite-T-cell combinations, in part, because for many parasites the number T cells did not vary over time or there were no T cells near the parasite. However, for eight parasites we found that T cell numbers in the cluster are negatively correlated with VI (**Figure 2**B) suggesting that at least for a subset of parasites CD8 T cells may suppress parasite's "health".

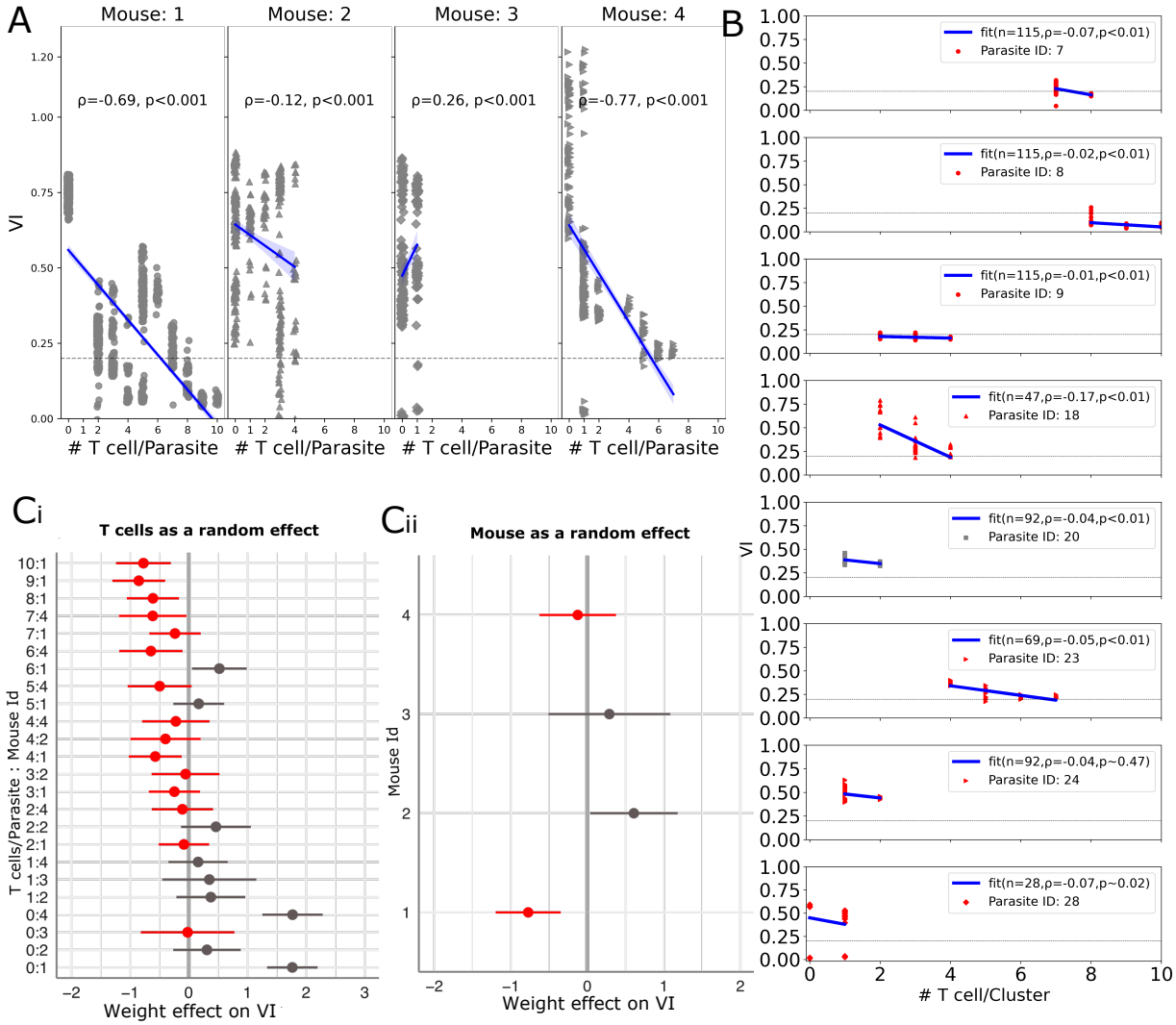

Figure 2: Higher CD8 T cell numbers per parasite are negatively correlated with the parasite's VI. (A) Correlation between parasite's VI and T cell numbers per parasite is shown for individual mice. The Spearman rank correlation coefficients ρ and corresponding p value were calculated using *scipy.stat* package in python and are shown on individual panels. (B) Correlation between parasite's VI and CD8 T cell numbers per parasite shown for subset of the data (8/32) for which such correlation was statistically significant (red and gray colors for the points correspond to dying and not dying parasites, respectively). Lines show linear regression with p value calculated using *statsmodels* package in python. (Ci) Prediction of the best fit linear mixed effects model assuming T cell numbers per parasite as a random effect (eqn. (11)) are shown for individual T cell number:mouse combinations. Negative values for effect (weight) correspond to T cell numbers that reduce VI over time. (Cii) Prediction of the best fit linear mixed effects model assuming mouse as a random effect (eqn. (10)) are shown for individual mice (negative and positive effect corresponds to the parasite's VI declining or increasing, respectively).

To understand how the time since T cell transfer may impact the relationship between T cell number per parasite and parasite's VI we fitted several alternative models to the parasite's VI normalized to its average value for each parasite for all mice but dividing the data into different time periods (see **Figure 1**Ciii, **Supplemental Figure S5**, and eqns. (1)–(5) in Materials and methods).

Specifically, we divided the VI and T cell data for 32 parasites into four different cohort based on the time interval since T cell transfer (4-6 hours, 6-8 hours, 8-11 hours, and all data combined, 4-11 hours) and fitted five alternative models (eqns. (1)–(5)) to these data using least squares. All models described the data with similar quality and model predictions were typically similar for the alternative models with the exception of the exponential model that gave slightly different predictions (**Supplemental Figure S5**A-C). For each time period we then calculated the number of T cells, T_{IC50}, that was needed to reduce parasite's VI to 50% of its initial value. Interestingly, T_{IC50} was increasing with the time since T cell transfer from about 1 T cell per parasite at early time points (4-6 hours) to 13 T cells per parasite at later time points (8-11 hours, **Supplemental Figure S5**A-C). This result may indicate that there may be something special about parasites that had survived for 8-11 hours of T cell search for infection; perhaps such parasites are able to actively resist killing or that they are located in areas of the liver where T cells have lower access to. When analyzing all the data together we found that about 3 Py-specific CD8 T cells per parasite were needed to reduce the parasite's VI to 50% of its initial value (**Supplemental Figure S5**D); this estimate of the cluster size is similar to that calculated previously using an alternative analysis [16].

Finally, to quantify the effect of the time since T cell transfer, the number of T cells per parasite, and the individual mouse we performed several linear mixed model-based analyses (see eqns. (6)–(13) and Materials and methods for more detail). By comparing among alternative models, the model in which VI was dependent on time since T cell transfer as a fixed effect and mouse being a random effect (eqn. (11)) described the data with best quality. In this model, based on total variance explained by the model the overall contribution of CD8 T cell number on parasite's VI was about 60% and mouse effect was about to 40%. Overall, higher T cell numbers were associated with decline in VI over time (**Figure 2**C); however, in mice 2&3 the VI did not significantly decline over time (**Figure 2**D). This analysis suggests that while CD8 T cell numbers per parasite do explain the dynamics of the parasite's VI (decline or growth), the effect is individual mouse-dependent highlighting the need to perform experiments in as many mice as possible.

3.3 A forecasting model with increasing T cell number per parasite better describes change in parasite's VI

Parasite's VI fluctuated over time for most parasites (e.g., **Figure 1**Bii). To investigate whether current VI and T cell number per parasite are predictive of the VI at a later time instance we borrowed an approach from economics dubbed "a forecasting model" (**Figure 3**Ai). We assumed how current and past VI are related, i.e., whether the next step VI is directly determined by the previous VI value eqns. (14)–(15) for the set of equations. In the model we then considered the impact of CD8 T cell number at the current time moment on the next time VI, and examined whether changes of T cell number per parasite improves the quality of the model fits of the VI data. We found that for T cell dynamics observed in experiments, adding T cell dynamics to the model fit improved the prediction of VI dynamics for 6 out of 19 parasites (**Figure 3**Bi).

We wondered if there may be errors in measuring of how many CD8 T cells are located near individual parasites. In our experiments the typical imaging depth is $h = 50$ μm, and given that we count T cells located within $r = 40$ μm from the parasite, the relative volume in which we typically count T cells near the deep parasite is $\pi r^2 h/(4/3\pi r^3) \approx 47\%$. This calculation suggests that we may be underestimating the number of T cells located near individual parasites, and it is possible that our determined change in T cell numbers per parasite may also be not fully accurate.

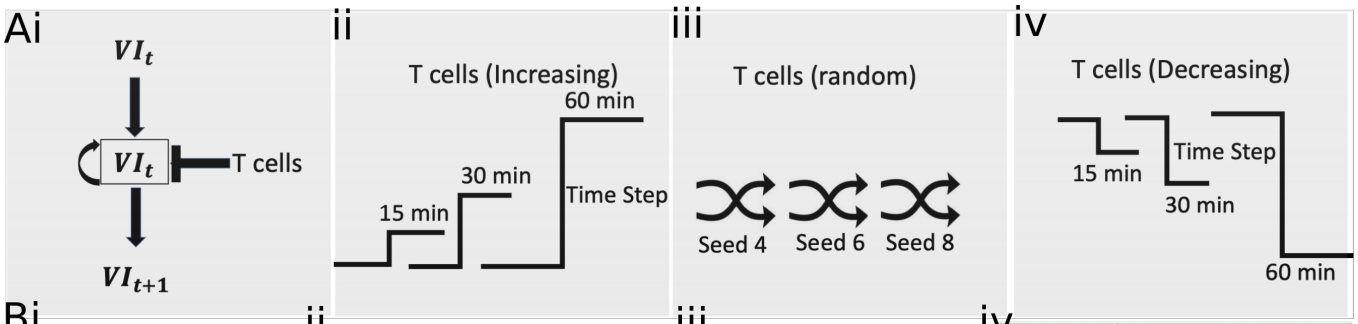

Bi

Parasite ID	Initial T-cells	Anova (T-cells Vs Null) Experimental Data
1	5	0.61423
3	3	0.04*
4	5	0.0093*
5	2	0.00125*
7	7	0.2958
8	8	4.3E-08*
9	2	0.00997*
12	2	0.15373
13	0	0.92808
14	0	0.15435
17	3	0.92243
18	2	0.3656
19	4	0.16019
20	1	0.18949
22	0	0.64907
23	4	0.01812*
24	1	4.0E-06#
27	0	0.782644
28	0	0.727104
Total p(<0.05):		6

ii

Anova(increasing T-cell Vs Null)		
Time Step – 15 mins	Time Step – 30 mins	Time Step – 60 mins
0.6322	0.4855	0.3521
0.0005*	0.0027*	0.0017*
0.000067*	0.00056*	0.00087*
0.001052*	0.00053*	0.0008*
0.15265	0.32379	0.32379
8.34E-08*	3.99E-08*	3.99*
0.0000069*	0.000241*	0.003374*
0.12057	0.08353	0.1133
0.81775	0.79196	0.80223
0.004304*	0.00775*	0.018011*
0.10183	0.03804*	0.14389
0.029696*	0.36807	0.011355*
0.06904	0.05713	0.33334
0.000659*	0.002135*	0.03764*
0.04583*	0.04629*	0.02934*
0.00001736*	0.0002045*	0.093003
0.00032*	0.00402*	0.0003*
0.02375*	0.03878*	0.04732*
0.28474	0.23267	0.4632
12	12	11

iii

Anova (random T-cells Vs Null)		
Random seed-4	Random seed-6	Random seed-8
0.8096	0.3373	0.7777
0.0139*	0.026*	0.0096
0.0016*	0.0001*	0.01324
0.49711	0.27092	0.55263
0.53662	0.3796	0.13458
1.2E-06*	7.9E-07*	7.3E-09
0.04596*	0.13934	0.064771
0.004107*	0.0079*	0.11538
0.97186	0.91301	0.50321
0.64246	0.36752	0.00031*
0.34309	0.90727	0.96746
0.041532*	0.11282	0.32452
0.00084*	0.93893	0.99029
0.074165	0.143268	0.471
0.71035	0.85236	0.51198
0.57018	0.416445	0.45454
0.07534	3.5E-05*	4.0E-05*
0.59685	0.601323	0.5958
0.52672	0.7521	0.72184
7	5	2

iv

Anova (decreasing T-cell Vs Null)		
Time Step – 15 mins	Time Step – 30 mins	Time Step – 60 mins
0.6034	0.6189	0.6275
0.3124	0.1298	0.0249*
0.3741	0.04533*	0.00297*
0.11941	0.0657	0.096
0.73672	0.54395	0.54395
2.8E-05*	8.6E-06*	8.6E-06*
0.39182	0.3536	0.08714
0.423535	0.054537	0.319363
NA	NA	NA
NA	NA	NA
0.27103	0.99999	0.4509
0.011356*	0.011355*	0.3985
0.000832*	0.23168	0.299577
0.06985	0.99999	0.047638*
NA	NA	NA
0.44328	0.50619	0.0009*
3.9E-05*	3.9E-05*	4.0E-05*
NA	NA	NA
NA	NA	NA
4	4	6

Figure 3: Increasing T cell numbers improves prediction of parasite's VI over time. (A) (i) Schematic diagram of the model to predict next VI (V_{t+1}) using its own previous value (V_t) and reduction of VI due to CD8 T cells present near the parasite. (ii) We increased the T cell number per parasite over time (with three different time steps) starting from the minimal number of T cells found for a given parasite to 10 – a maximum value observed in our data (see **Supplemental Figure S4** for the dynamics of T cell number for each parasite). (iii) We supplied a random T cell number over time (using three different random seeds) that were bounded by lowest and highest T cell number taken from experimental data. (iv) We decreased the T cell number over time (with three different time step) starting from the highest T cell number found in experiments for each parasite to zero. (B) We compared the fits of the forecasting null model where the next time step VI is only determined by the VI at the current step (eqn. (14)) with the model in which the dynamics of CD8 T cell numbers is included (eqn. (15)) using ANOVA in R. In fitting the model with changing CD8 T cell numbers per parasite we (i) took the actual T cell number data for each parasite, (ii) increased CD8 T cell numbers over time, (iii) chose random T cell numbers over time, and (iv) decreased T cell numbers over time. The analysis was done for 19 parasites for which there was at least 1 T cell nearby at several time points during the imaging period. Red and gray shading of rows denotes parasites that are dying (VI has declined or is declining to 0.2) or not dying, respectively. "NA" denotes situation when T cell number was zero. Linear regressions were done in R package *minpack.lm* with star $*$ denoting statistically significant difference in model fits at $p < 0.05$. Estimated model parameters are shown in **Supplemental Table S2**.

To investigate whether different T cell dynamics may improve prediction of the VI changes over time we simulated T cell dynamics for each parasite in three different ways: we assumed that 1) T cell number per parasite increases with time since T cell transfer from the minimal value found for a given parasite to 10 (maximum observed in our data), 2) T cell number is randomly chosen between minimal and maximal value, or 3) T cell number declines from the maximal value over time to zero. We found that increasing the number of T cells over time improves the description of the VI dynamics over the null model with no T cells in 12/19 parasites – a double when compared to the model fits when using actual data ($\chi_1 = 2.64$, $p = 0.10$; **Figure 3**Bii). This result was relatively independent on the rate at which T cell numbers were assumed to increase over time. In contrast, choosing random T cell numbers or decreasing T cell numbers over time resulted in fewer fits that improved prediction of parasite's VI over the null model (**Figure 3**Biii-Biv). These results suggest that there may be an increase in the number of T cells around individual parasites that is not fully detectable by the current imaging techniques at least for some (e.g., deep) parasites.

3.4 A simple model with mass action killing describes well the VI dynamics for a subset of the data

Having performed several statistical analyses of the data we next turned to a more mechanistic modeling of T cell-mediated killing of the parasites by asking whether the kinetics of VI loss over time can be well described by different mathematical models. We focused this analysis on the subset of parasites for which we found a statistically significant negative correlation between VI and T cell number (**Figure 2**B). First, we quantified the kinetics of CD8 T cell accumulation for each of these parasites over time using our previously developed "density-dependent recruitment" (DDR) model (eqn. (16)). Specifically, we fitted the model (eqn. (16)) to the measured numbers of CD8 T cells per parasite using nonlinear least squares and estimated model parameters (λ_0 and $\mu - \lambda_1$, **Supplemental Figure S6**). Both parameters varied dramatically between individual parasites (e.g., from minimal $\lambda_0 = 0.016$/h to maximal $\lambda_0 = 3.36$/h values), but, overall, the model could accurately describe T cell clustering dynamics.

We then compared how well three alternative models that assume different killing terms and that use the estimated dynamics of T cell numbers per parasite, fit the data on the dynamics of parasite's VI (**Figure 4**A). Specifically, we fitted the models assuming 1) mass-action killing rate (eqn. (17)), 2) powerlaw killing term (eqn. (18)), or 3) Hill-like killing term (eqn. (19)) to the change in VI over time using nonlinear least squares. In the fits we assumed that the parasite's growth rate $r = 0$ since our analysis of the data on VI dynamics in control mice found that this growth rate on average was not different from zero. (Fitting the models assuming $r > 0$ resulted in overfitting). We found that in all but one case, the model assuming mass-action killing term described the data with sufficient quality, and increasing model complexity did not improve the model fit of the data based on AIC (**Figure 4**B-I and results not shown). Only for one parasite (ID=28) we found that a powerlaw model in which CD8 T cells cooperate in killing ($n = 8$) described the data with improve quality (**Figure 4**I). Ironically, only a single T cells came into close proximity to the parasite for a period of time and then left (**Supplemental Figure S4**). High n was selected in the fit because of the very rapid decline in VI with a single T cell coming in contact with the liver stage — an interesting example of a lethal hit being delivered rapidly. Interestingly, the estimated kill rates k did not vary dramatically between individual parasites with the average kill rate being $\bar{k} = 0.068$/h (**Figure 4** and **Supplemental Table S3**). Importantly, the estimated per capita kill rate did not depend on the average number of T cells per parasite (t-test, $p = 0.47$) further supporting the mass-action killing

model.

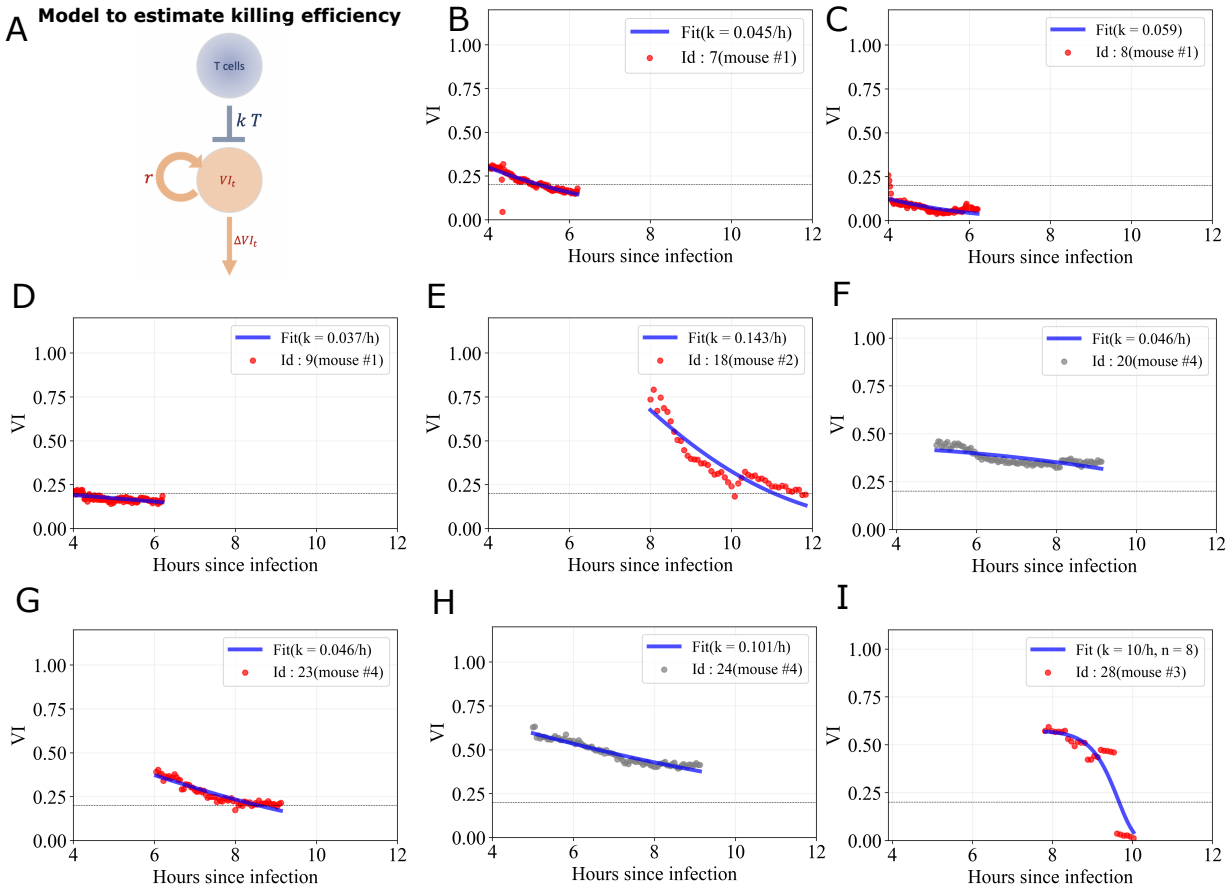

Figure 4: The best fit model suggests a relatively low killing efficacy of CD8 T cells in vivo. (A) Schematic of the model depicting the essential interaction between CD8+ T cells (T) and VI (V_t) where k, r, and n correspond to killing efficiency per T cell, growth rate of the parasites, and parameter indicating competition ($n < 1$) or cooperation ($n > 1$) between T cells located near the same parasite, respectively. Three alternative models (eqns. (17)–(19)) were fitted to the data on VI dynamics while taking into account change in the number of CD8 T cells per parasite as predicted by the density-dependent recruitment model (**Supplemental Figure S6**). (B-I) Experimental data on VI change in subset of parasites are shown by markers and lines are the best fit predictions of the simplest, mass-action model (eqn. (17)). Estimated killing rate k is shown on individual panels and other parameters are shown in **Supplemental Table S3**. Coloring of the data (red or gray) represents dying or non-dying parasites, respectively. The dotted horizontal line denotes the death threshold VI = 0.2.

It was possible that deviations of the killing from mass-action was not detectable in the data for individual parasites. Therefore, we fitted the alternative models (eqns. (17)–(18)) to the VI data for 8 parasites in **Figure 4** using non-linear mixed effect modeling approach (by using `nlme` function in `R`). Surprisingly, we found that allowing both killing rate k and the initial VI ($\log V0$) to vary between parasites fitted the data significantly better than the model in which the killing rate k was set as a fixed effect or when all parameters were assumed to have only fixed effects (likelihood ratio test, $p < 0.001$). This precluded us from finding a kill rate that would allow the model to describe well the VI dynamics for this subset of the data. We found a similar conclusion when fitting the models to data on VI dynamics for all 32 parasites.

To more robustly estimate the CD8 T cell killing rate from these data we fitted the mass-action killing model (eqn. (17)) to the VI dynamics for all parasites in the subset of data ($n = 8$) using a Bayesian approach. The model fit suggested the per capita killing rate of CD8 T cells of $k = 0.049$/h corresponding to the half-life of 14.2 hours (**Supplemental Figure S7**) which is slightly lower than

the average value found by nonlinear least squares fits of the model to data for individual parasites. Importantly, alternative models that assume deviations from mass-action killing (e.g., eqns. (18)–(19)) did not describe the data with better quality (based on Bayesian Information criterion, BIC) further supporting the conclusion that CD8 T cells act independently at killing Py liver stages in mice. Given that it is typical for the parasite's VI to be one at the start of imaging (e.g., **Figure 1**Bi) and that VI = 0.2 was considered to correspond to a dead/dying parasite [16], a single T cell will need on average $-\ln(0.2)/k = 33$ h to eliminate the infection. Because it may take hours for T cells to locate the infection [31], this analysis suggests that while a single Py-specific CD8 T cell is able to kill the parasite, multiple CD8 T cells may be needed for efficient location and elimination of the parasite in the 48 hours of the liver stage lifespan.

3.5 Stochastic model with independent and random T cell response is unable to explain the stability of VI most parasites

In our set of 32 parasites many parasites displayed no evidence of declining VI despite being surrounded by one or several CD8 T cells for a period of time (e.g., parasite ID 11 and 12 in **Supplemental Figure S2**). Given that the estimated killing rate of CD8 T cells was relatively low (**Figure 4**) we hypothesized if constant VI could be explained simply by insufficient imaging period of a few hours preventing us to see a noticeable decline in the VI.

To test this hypothesis we performed stochastic simulations of the parasite's GFP signal that would mimic our experimental design (see Materials and methods for detail). We started the simulation with the parasite's GFP signal being 100 that could change up or down by one (similar to information provided in the imaging data) and then calculated parasite's VI assuming background of one (i.e., the initial VI was $\log_{10}(100/1) = 2$). We allowed the parasite's VI to grow for 20 hours with a small growth rate $r = 0.0001$/h. After 20 hours T cells were transferred into the mice and started forming clusters around the parasite – the number of T cells per parasite was given by eqn. (16) with parameters chosen for individual parasites (**Supplemental Figure S6**). We started recording the VI 4-8 hours after T cell transfer and continued for another 2-4 hours. T cells were assumed to reduce the VI according to the mass action model with $k = 0.049$/h. In this way we simulated 250 trajectories and estimated the rate at which VI was declining with time for individual runs taking the time period of imaging into account (**Figure 5**). The VI for individual runs was typically declining with time whether few or many T cells were located near the parasite (**Figure 5**A&C) even though there was large variability in the decline rates (**Figure 5**B&D). Importantly, none of the slopes of VI decline in simulations were close to the slow VI decline rate observed in the data for "non-dying" parasites. We also performed stochastic simulation with random CD8 T cells number within the specific range of per parasite data. But our simulation slope fails to capture the VI slope observed experimentally (**Supplemental Figure S8**). That suggests that our hypothesis that stable VI is due to stochasticity in the VI dynamics is not consistent with the data. The reasons why some parasites remain viable with no evidence of declining VI despite being surrounded by T cells remain unclear but may include at least three alternative explanations: 1) while being close, Py-specific CD8 T cells do not recognize the infection, 2) the parasite was actively inhibiting killing signals that CD8 T cells may be delivering to the infected cell, and 3) CD8 T cells in the cluster are unable to kill the parasite due to lack of the killing-related molecules (e.g., perforin/granzymes).

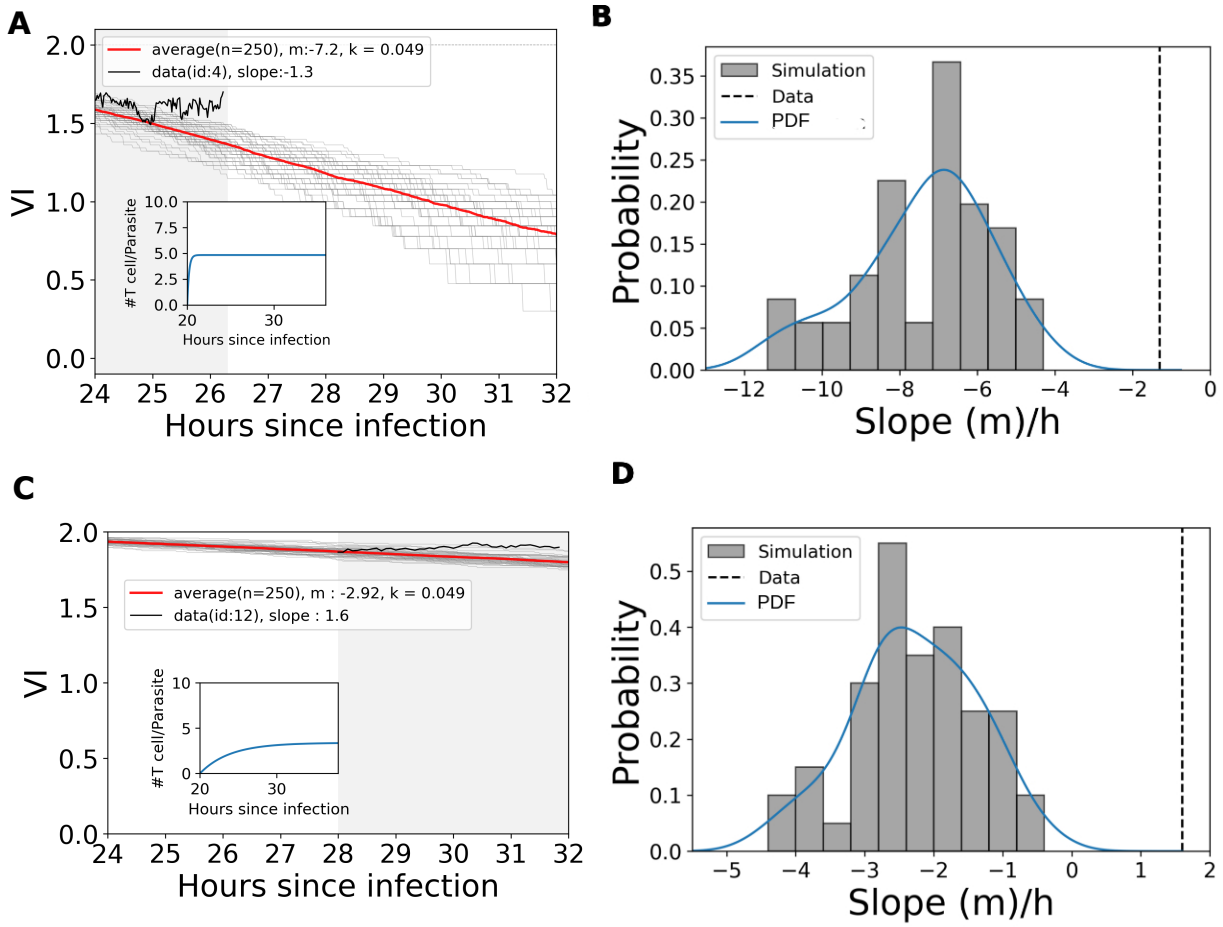

Figure 5: Constancy of parasite's VI is not consistent with stochastic simulations of killing by T cells. We simulated parasite's VI dynamics using Gillespie algorithm for 20 hours with a small growth rate $r = 0.0001/\text{h}$ and then added killing by T cells at a per capita rate $k = 0.049/\text{h}$ with the total kill rate being determined by the total number of T cells per parasite increasing with time (see Materials and methods for more detail). **A, C**: We plot trajectory from 250 simulations (gray lines) with the average change (red line) calculated from every time step of 0.02 hour. T cell dynamics was added in the simulations using eqn. (16) with parameters estimated for individual parasites (A-B: ID4, C-D: ID12). Black lines in panels A&C show the actual change in VI over time as was observed in the data for parasite IDs 4 (A) and 12 (C). **B, D**: For every simulation we calculate the decay rate of the VI and show the distribution of decay rate with probability density function (blue line). The actual decay rate for the VI in the data for these two parasites (ID4 and ID12) is shown by horizontal black dotted line. Inserts show the T cell dynamics as assumed by the clustering model. Gray shaded area denote the imaging period which we used to calculate the VI decay rate. Simulations were done using package *gillespy2* with *Tau-Hybrid solver* in python. None of VI slopes in simulations were above the VI slope in the data suggesting $p < 0.01$ for the comparing simulations with the data.

4 Discussion

It is well established that large numbers of Plasmodium-specific CD8 T cells are able to provide sterilizing protection against exposure to Plasmodium sporozoites but the mechanisms by which these T cells eliminate the parasites in the liver remain unclear. We used data from our previous intravital imaging of livers in live mice to accurately quantify kinetics at which Py-specific CD8 T cells eliminate Py parasites from the liver [16]. In several alternative statistical analyses we found that presence of Py-specific CD8 T cells typically results in a faster loss of the VI signal from the parasites that we interpret as the process of parasite's dying. We estimated that on average 3 T cells per parasite are needed to reduce the parasite's VI to 50% of its initial value during the imaging period ($\sim$ 4 h), and that the dynamics of VI is better explained by the model in which the number of T cells per parasite steadily increases over time (**Supplemental Figure S5** and **Figure 3**). Analysis of the subset of data – the parasites for which the VI and CD8 T cell numbers were negatively correlated – suggested that T cells reduce the VI at a relatively slow per capita rate ($k = 0.049$/h, **Figure 4**) suggesting that a single T cell may be able to eliminate the infection (reduce VI from 100 to 20%) within 48 hours of the parasite's lifespan if it can find the infection quickly. There was large heterogeneity in the kinetics of VI decline between individual parasites; the rate of VI decline only weakly correlated with the number of T cells present near the parasite (**Supplemental Figure S9**), and VI of many parasites surrounded by several CD8 T cells remained relatively constant during the imaging. Stochastic simulations of the VI dynamics in presence of different numbers of T cells suggested that constancy of the VI over the observation period cannot be due to limited duration of imaging (**Figure 5** and **Supplemental Figure S8**). Instead, it is likely that while clustering of T cells around the parasites is driven by chemotactic cues [22, 31] either clustered CD8 T cells do not have direct access to the infected hepatocyte, do not recognize the infected cell, lack killing machinery, or that the parasite has means to actively resist killing.

Details of how individual CD8 T cells kill their targets in vivo remain poorly understood, in part of difficulty of recording killing events in live animals. Several studies reported that CD8 T cells are able to kill either peptide-pulsed or virus-infected cells in 1-2 hours after initial contact [14, 17]. It may take longer times, about 6 hours, for a CD8 T cell to kill a cancer cell [15] although a recent study suggests a faster kill rate of B16 cancer cells by CD8 T cells in vivo [19]. Yet, all these estimates of kill rates are faster than what we found in our study suggesting that the type of target cell (e.g., type of intracellular pathogen) and of the tissue may influence the killing ability of T cells. One previous study found evidence of T cell cooperativity in killing of virus-infected cells [17], although a later re-analysis of the same imaging data suggested additive (mass-action like) killing by T cells [18]. Linear/additive effect of killing was also proposed in another study where delivery of 3 independent lethal hits by the same or different T cells within a short time period (< 1 h) was associated with target cell death [19]. We also did not find any evidence of T cell cooperation at elimination of Plasmodium liver stages but when multiple T cells cluster around the parasite, the probability of the parasite's death during the imaging period was higher (**Figure 2**Ci).

Many studies have estimated the rate at which a population of antigen-specific CD8 T cells kill their targets in vivo, for example, by using in vivo cytotoxicity assay (e.g., [32–35]), with target cell death rates ranging from minutes to days (reviewed in [36]). The exact reasons for this variability have not been fully elucidated but may involve differences in type of target cells used in experiments, how T cell antigens are expressed by the targets (e.g., peptide-pulsed vs infected), and variability in individual T cells in their killing ability. Indeed, several recent reports by tracking individual CD8 T cells suggested great variability of antigen-specific T cells in ability to kill their targets

[17, 19]; variability in ability of different T cells to kill targets in vitro has been also well documented [19, 37, 38].

Our study has several limitations. To track viability of the Plasmodium liver stages we imaged a relatively small area around the parasite ($\sim 200 \times 200 \times 50$ μm) and T cells within 40 μm of the parasite were considered to be close to the infected hepatocyte for killing [22]. For the parasites located at the deeper liver areas (with a higher z-coordinate), we may have underestimated the number of clustered T cells. Indeed, artificially increasing the number of clustered T cells improved the model prediction on the VI dynamics supporting the idea that there may have been more clustered T cells than that observed experimentally. To more accurately evaluate how Plasmodium-specific CD8 T cells eliminate the infection our experiments were performed in "reverse": mice were first infected, T cell transferred only 20 hours after the infection and imaging was done several hours after the T cell transfer (**Figure 1**A). In part, this was also done due to low GFP expression by individual Py sporozoites that did not allow imaging of individual parasites from the start of infection. This setup corresponds to cases of adoptive T cell transfer therapy against cancer and not to prophylactic vaccination when activated/memory T cells are typically present prior to infection. Whether killing of Plasmodium liver stages proceeds similarly in cases when T cells are present in mice prior to infection and when sporozoites just invade the liver remains to be investigated.

While we have estimated that T cells reduced the parasite's VI at a rate of $k = 0.049$/h (or $\bar{k} = 0.068$/h) whether this is a lower or upper bound estimate is not entirely clear. Because in our experiments imaging started few hours after T cell transfer, our analysis may underestimate the T cell killing efficiency if killing occurs at a higher rate when T cells just locate the parasite. At least for a subset of parasites for which there was a consistent decline in VI over time our estimates of the killing rate should be relatively robust to the assumption of early killing. On the other hand, many parasites showed no evidence of dying despite being surrounded by several T cells suggesting that estimated killing efficacy may be an overestimate. Because our imaging protocol required to observe GFP signal from the parasite, some parasites may have been killed by T cells prior to imaging start, thus, creating a bias towards detecting parasites that are not being killed fast. Indeed, we found that more T cells are needed to reduce the VI to 50% of its initial value at later times after T cell transfer (**Supplemental Figure S5**) supporting potential existence of such bias.

It was interesting and surprising to record that the majority of the liver stages in our experiments displayed no evidence of dying (i.e., no reduction in VI over time) despite being surrounded by several Plasmodium-specific T cells. The exact reasons for that remain to be determined. In particular, clustered T cells could differ in their killing ability [19, 37], may not have access to the infected hepatocyte, or that the parasite was simply able to resist the killing. For example, a recent study suggested that several hits may be needed to kill a cancer cell [19] which implies that some cancer cells may actively resist killing [39].

Because the number of T cells clustered near individual parasites varied over time to estimate T cell killing rates we needed a model to describe clustering dynamics. We used our previously suggested density-dependent recruitment (DDR) model for that purpose, in part, because it was the best model for the clustering data [22]. In our analysis we used constant, time-independent parameters for the DDR model which fitted the data well (**Supplemental Figure S6**); however, our recent analysis suggested that the DDR model parameters are likely to decline over time [22]. Because in model fitting to VI data we only used the average number of T cells per parasite, the specific details of why clusters reach a particular size is not important; yet, future studies may need to investigate whether modeling cluster formation using so-called "longitudinal data", when change

in the number of clustered T cells is modelled probabilistically [22, 40], yields different estimates of the killing rates.

Several in vitro studies suggested that CD8 T cells are able to serially kill their targets [41–44]. Because we typically followed individual parasites located in different areas of the liver we could not document if T cells in these experiments performed serial killing. In fact, given seemingly random search of most T cells for the liver stages [31], sparcity of infected hepatocytes in the liver even at high infection doses, and relatively long time it takes for T cells to kill the parasite, it is unlikely that serial killing is relevant to CD8 T cell-mediated elimination of Plasmodium liver stages in mice.

Our estimate that even a single cell should be able to kill a liver stage within 48 hours of its lifespan based on the assumption that decline of the VI from 1 to 0.2 will result in parasite's death [16]. However, the death threshold VI = 0.2 may not be accurate for all parasites; better understanding at what VI level parasites die and potential causes of VI variability may allow for more accurate prediction of the time it takes for T cells to eliminate the infection from the liver.

Our study opens up directions for future research. Details of T cell clustering around individual liver stages remain incompletely understood. While previously we found a strong support for the DDR model [22] our inability to find evidence of attraction of most T cells towards the infection site is troubling [31]. One recent study also suggested a potential role of recirculating T cells in control of infection with Plasmodium sporozoites [45], and T cells may be following attracting cues via the liver sinusoids rather than via direct, Euclidean distance-based search as we have assumed previously [31]. Developing rigorous frameworks of how T cells search for the infection via the sinusoids is an active area of our research. Several cytokines such as IFNg and chemokine receptors (e.g., CXCR3, CCR5, and others) have been shown to be important in T cell-mediated control of Plasmodium infection [11, 46]. The role of these molecules in the efficiency of T cell search for and elimination of Plasmodium liver stages remains to be investigated. Future studies will need to combine the estimates of times it takes for CD8 T cells to locate and then to kill the liver stage. While several studies have found bias in T cell movement towards an infection site [47, 48], we failed to do so for most T cells in the liver even using a more sensitive metric to detect attraction [31]. In the absence of attracting cues the time to find the infection site may be substantial [11, 31] further reducing a chance that a single T cell is always able to eliminate a liver stage.

Taken together, our analyses indicate that the average ability of CD8 T cells to kill Plasmodium liver stages is rather limited and is not in agreement with the conclusion that activated CD8 T cell act as "rapid" and "serial" killers that destroy hundreds or thousands of targets per day [36]. Deeper understanding of factors that contribute to the ability of T cells to kill their targets – such as the dynamics of CD8 T cell response, heterogeneity of CD8 T cells populations, T cell recirculation/migration kinetics, and specific details of the tissues where T cells encounter their targets [49] – are likely to improve our ability to estimate T cell kill rates and to make more accurate predictions on the number of T cells required to control infections and cancers [50]. Ultimately, better experimental methods, for example those using Ca-flux mice allowing to visualize recognition of antigen by T cells (and thus potentially, the delivery of the lethal hit) [19], will provide more a sophisticated description of how CD8 T cells kill their targets in vivo.

Data availability

The data used in the analysis are provided as a supplement to the paper as well as on github along with computer codes: https://github.com/soumenbera89/Killing-of-Malaria-Parasite-by-CD8-T-cell

Code availability

We performed most of our analyses in python and provided several key codes to ensure reproducibility of our results on github: https://github.com/soumenbera89/Killing-of-Malaria-Parasite-by-CD8-T-cell

Author's contributions

The data for the analyses have been generated in previous study primarily by IAC and RA. RA also contributed previously unpublished changes in the vitality index of Py liver stages in control experiments. VVG and SB designed some of the quantitative analyses including formulation of mathematical models. Most analyses have been performed by SB. IAC provided feedback on the analyses performed. SB wrote the first draft of the paper which was then edited by all authors. All authors contributed to writing the final version of the paper.

Acknowledgements

This work was supported mainly by R01GM118553 and partially by R01AI158963 NIH awards to VVG.

References

1. Organization, W. H. *et al.* 2021 World malaria report 2021.

2. Aleshnick, M., Ganusov, V. V., Nasir, G., Yenokyan, G. & Sinnis, P. 2020 Experimental determination of the force of malaria infection reveals a non-linear relationship to mosquito sporozoite loads. *PLoS pathogens*, **16**, e1008 181. doi:10.1371/journal.ppat.1008181.

3. Amino, R., Thiberge, S., Martin, B., Celli, S., Shorte, S., Frischknecht, F. & Ménard, R. 2006 Quantitative imaging of Plasmodium transmission from mosquito to mammal. *Nat Med*, **12**(2), 220–224. doi:10.1038/nm1350.

4. Schmidt, N. W., Podyminogin, R. L., Butler, N. S., Badovinac, V. P., Tucker, B. J., Bahjat, K. S., Lauer, P., Reyes-Sandoval, A., Hutchings, C. L. *et al.* 2008 Memory CD8 T cell responses exceeding a large but definable threshold provide long-term immunity to malaria. *PNAS*, **105**(37), 14 017–14 022.

5. Ishizuka, A. S., Lyke, K. E., DeZure, A., Berry, A. A., Richie, T. L., Mendoza, F. H., Enama, M. E., Gordon, I. J., Chang, L.-J. *et al.* 2016 Protection against malaria at 1 year and immune correlates following PfSPZ vaccination. *Nature medicine*, **22**(6), 614–623.

6. Kurup, S. P., Butler, N. S. & Harty, J. T. 2019 T cell-mediated immunity to malaria. *Nature Reviews Immunology*, **19**(7), 457–471.

7. Romero, P., Maryanski, J. L., Corradin, G., Nussenzweig, R. S., Nussenzweig, V. & Zavala, F. 1989 Cloned cytotoxic T cells recognize an epitope in the circumsporozoite protein and protect against malaria. *Nature*, **341**(6240), 323–326. doi:10.1038/341323a0.

8. Schmidt, N. W., Butler, N. S., Badovinac, V. P. & Harty, J. T. 2010 Extreme CD8 T cell requirements for anti-malarial liver-stage immunity following immunization with radiation attenuated sporozoites. *PLoS Pathog*, **6**(7), e1000 998. doi:10.1371/journal.ppat.1000998.

9. Schmidt, N. W., Butler, N. S. & Harty, J. T. 2011 Plasmodium–host interactions directly influence the threshold of memory cd8 t cells required for protective immunity. *The Journal of Immunology*, **186**(10), 5873–5884.

10. Epstein, J. E., Tewari, K., Lyke, K. E., Sim, B. K. L., Billingsley, P. F., Laurens, M. B., Gunasekera, A., Chakravarty, S., James, E. R. *et al.* 2011 Live attenuated malaria vaccine designed to protect through hepatic CD8 T cell immunity. *Science*, **334**(6055), 475–480. doi: 10.1126/science.1211548.

11. Fernandez-Ruiz, D., Ng, W. Y., Holz, L. E., Ma, J. Z., Zaid, A., Wong, Y. C., Lau, L. S., Mollard, V., Cozijnsen, A. *et al.* 2016 Liver-resident memory CD8(+) T cells form a front-line defense against malaria liver-stage infection. *Immunity*, **45**, 889–902. doi:10.1016/j.immuni.2016.08.011.

12. Draper, S. J., Sack, B. K., King, C. R., Nielsen, C. M., Rayner, J. C., Higgins, M. K., Long, C. A. & Seder, R. A. 2018 Malaria vaccines: Recent advances and new horizons. *Cell host microbe*, **24**, 43–56. doi:10.1016/j.chom.2018.06.008.

13. Lyke, K. E., Ishizuka, A. S., Berry, A. A., Chakravarty, S., DeZure, A., Enama, M. E., James, E. R., Billingsley, P. F., Gunasekera, A. *et al.* 2017 Attenuated PfSPZ vaccine induces strain-transcending T cells and durable protection against heterologous controlled human malaria infection. *Proc Natl Aca*, **114**, 2711–2716. doi:10.1073/pnas.1615324114.

14. Mempel, T., Pittet, M., Khazaie, K., Weninger, W., Weissleder, R., von Boehmer, H. & von Andrian, U. 2006 Regulatory T cells reversibly suppress cytotoxic T cell function independent of effector differentiation. *Immunity*, **25**(1), 129–41.

15. Breart, B., Lemaitre, F., Celli, S. & Bousso, P. 2008 Two-photon imaging of intratumoral CD8+ T cell cytotoxic activity during adoptive T cell therapy in mice. *J Clin Invest*, **118**(4), 1390–7.

16. Cockburn, I. A., Amino, R., Kelemen, R. K., Kuo, S. C., Tse, S.-W., Radtke, A., MacDaniel, L., Ganusov, V. V., Zavala, F. *et al.* 2013 In vivo imaging of CD8+ T cell-mediated elimination of malaria liver stages. *Proc Natl Acad Sci U S A*, **110**(22), 9090–9095. doi: 10.1073/pnas.1303858110.

17. Halle, S., Keyser, K. A., Stahl, F. R., Busche, A., Marquardt, A., Zheng, X., Galla, M., Heissmeyer, V., Heller, K. *et al.* 2016 In vivo killing capacity of cytotoxic T cells is limited and involves dynamic interactions and T cell cooperativity. *Immunity*, **44**(2), 233–245.

18. Rastogi, A., Robert, P. A., Halle, S. & Meyer-Hermann, M. 2020 Evaluation of CD8 T cell killing models with computer simulations of 2-photon imaging experiments. *PLoS Comput Biol*, **16**, e1008 428. doi:10.1371/journal.pcbi.1008428.

19. Weigelin, B., den Boer, A. T., Wagena, E., Broen, K., Dolstra, H., de Boer, R. J., Figdor, C. G., Textor, J. & Friedl, P. 2021 Cytotoxic T cells are able to efficiently eliminate cancer cells by additive cytotoxicity. *Nature communications*, **12**(1), 1–12.

20. Morales-Navarrete, H., Segovia-Miranda, F., Klukowski, P., Meyer, K., Nonaka, H., Marsico, G., Chernykh, M., Kalaidzidis, A., Zerial, M. *et al.* 2015 A versatile pipeline for the multi-scale digital reconstruction and quantitative analysis of 3D tissue architecture. *Elife*, **4**, e11 214.

21. Severgnini, M., Sherman, J., Sehgal, A., Jayaprakash, N. K., Aubin, J., Wang, G., Zhang, L., Peng, C. G., Yucius, K. *et al.* 2012 A rapid two-step method for isolation of functional primary mouse hepatocytes: cell characterization and asialoglycoprotein receptor based assay development. *Cytotechnology*, **64**(2), 187–195.

22. Kelemen, R. K., Rajakaruna, H., Cockburn, I. A. & Ganusov, V. V. 2019 Clustering of activated CD8 T cells around malaria-infected hepatocytes is rapid and is driven by antigen-specific cells. *Frontiers in immunology*, **10**, 2153.

23. Ritz, C., Baty, F., Streibig, J. C. & Gerhard, D. 2015 Dose-response analysis using R. *PloS one*, **10**(12), e0146 021.

24. Akaike, H. 1974 A new look at the statistical model identification. *IEEE transactions on automatic control*, **19**(6), 716–723.

25. Burnham, K. P. & Anderson, D. R. 2002 A practical information-theoretic approach. *Model selection and multimodel inference*, **2**.

26. Bjørnstad, O. N., Finkenstädt, B. F. & Grenfell, B. T. 2002 Dynamics of measles epidemics: estimating scaling of transmission rates using a time series SIR model. *Ecological monographs*, **72**(2), 169–184.

27. Moré, J. J. 1978 The Levenberg-Marquardt algorithm: implementation and theory. In *Numerical analysis*, pp. 105–116. Springer.

28. Salvatier, J., Wiecki, T. V. & Fonnesbeck, C. 2016 Probabilistic programming in python using pymc3. *PeerJ Computer Science*, **2**, e55.

29. Gillespie, D. T. 1977 Exact stochastic simulation of coupled chemical reactions. *The journal of physical chemistry*, **81**(25), 2340–2361.

30. Goswami, D., Betz, W., Locham, N. K., Parthiban, C., Brager, C., Schäfer, C., Camargo, N., Nguyen, T., Kennedy, S. Y. *et al.* 2020 A replication-competent late liver stage-attenuated human malaria parasite. *JCI insight*, **5**. doi:10.1172/jci.insight.135589.

31. Zenkov, V. S., O'Connor, J., Cockburn, I. A. & Ganusov, V. V. 2022 A new method based on the von Mises-Fisher distribution shows that a minority of liver-localized CD8 T cells display hard-to-detect attraction to Plasmodium-infected hepatocytes. *Frontiers in Bioinformatics*, pp. 1–15. doi:10.3389/fbinf.2021.770448.

32. Barchet, W., Oehen, S., Klenerman, P., Wodarz, D., Bocharov, G., Lloyd, A. L., Nowak, M. A., Hengartner, H., Zinkernagel, R. M. *et al.* 2000 Direct quantitation of rapid elimination of viral antigen-positive lymphocytes by antiviral CD8(+) T cells in vivo. *Eur J Immunol*, **30**(5), 1356–1363.

33. Regoes, R., Barber, D., Ahmed, R. & Antia, R. 2007 Estimation of the rate of killing by cytotoxic T lymphocytes in vivo. *Proc Natl Acad Sci USA*, **104**(5), 1599–1603.

34. Ganusov, V. V. & De Boer, R. J. 2008 Estimating in vivo death rates of targets due to CD8 T-cell-mediated killing. *Journal of Virology*, **82**(23), 11 749–11 757.

35. Ganusov, V. V., Barber, D. L. & De Boer, R. J. 2011 Killing of targets by CD8 T cells in the mouse spleen follows the law of mass action. *PLoS One*, **6**(1), e15 959.

36. Elemans, M., Seich al Basatena, N.-K. & Asquith, B. 2012 The efficiency of the human cd8+ t cell response: how should we quantify it, what determines it, and does it matter? *PLoS computational biology*, **8**(2), e1002 381.

37. Varadarajan, N., Julg, B., Yamanaka, Y. J., Chen, H., Ogunniyi, A. O., McAndrew, E., Porter, L. C., Piechocka-Trocha, A., Hill, B. J. *et al.* 2011 A high-throughput single-cell analysis of human CD8+ T cell functions reveals discordance for cytokine secretion and cytolysis. *The Journal of clinical investigation*, **121**(11).

38. Vasconcelos, Z., Müller, S., Guipouy, D., Yu, W., Christophe, C., Gadat, S., Valitutti, S. & Dupré, L. 2015 Individual human cytotoxic T lymphocytes exhibit intraclonal heterogeneity during sustained killing. *Cell Reports*, **11**(9), 1474–1485.

39. Tuomela, K., Ambrose, A. R. & Davis, D. M. 2022 Escaping death: How cancer cells and infected cells resist cell-mediated cytotoxicity. *Frontiers in immunology*, **13**, 867 098. doi: 10.3389/fimmu.2022.867098.

40. Rajakaruna, H. & Ganusov, V. V. 2022 Evaluating impact of experimental design on accuracy of parameter estimation and model selection efficiency: T cell clustering as a case study. *BioRxiv*. doi:https://doi.org/10.1101/2022.03.30.486434.

41. Bossi, G., Trambas, C., Booth, S., Clark, R., Stinchcombe, J. & Griffiths, G. M. 2002 The secretory synapse: the secrets of a serial killer. *Immunological reviews*, **189**(1), 152–160.

42. Petrovas, C., Mueller, Y. M. & Katsikis, P. D. 2004 HIV-specific CD8+ T cells: serial killers condemned to die? *Current HIV research*, **2**(2), 153–162.

43. Wiedemann, A., Depoil, D., Faroudi, M. & Valitutti, S. 2006 Cytotoxic T lymphocytes kill multiple targets simultaneously via spatiotemporal uncoupling of lytic and stimulatory synapses. *Proceedings of the National Academy of Sciences*, **103**(29), 10 985–10 990.

44. Halle, S., Halle, O. & Förster, R. 2017 Mechanisms and dynamics of T cell-mediated cytotoxicity in vivo. *Trends in immunology*, **38**(6), 432–443.

45. Lefebvre, M. N., Surette, F. A., Anthony, S. M., Vijay, R., Jensen, I. J., Pewe, L. L., Hancox, L. S., Van Braeckel-Budimir, N., van de Wall, S. *et al.* 2021 Expeditious recruitment of circulating memory CD8 T cells to the liver facilitates control of malaria. *Cell Reports*, **37**, 109 956. doi: 10.1016/j.celrep.2021.109956.

46. Rodrigues, M., Nussenzweig, R. S. & Zavala, F. 1993 The relative contribution of antibodies, CD4+ and CD8+ T cells to sporozoite-induced protection against malaria. *Immunology*, **80**(1), 1–5.

47. Hickman, H. D., Reynoso, G. V., Ngudiankama, B. F., Cush, S. S., Gibbs, J., Bennink, J. R. & Yewdell, J. W. 2015 CXCR3 chemokine receptor enables local CD8+ T cell migration for the destruction of virus-infected cells. *Immunity*, **42**(3), 524–537.

48. Ariotti, S., Beltman, J. B., Borsje, R., Hoekstra, M. E., Halford, W. P., Haanen, J. B., de Boer, R. J. & Schumacher, T. N. 2015 Subtle CXCR3-dependent chemotaxis of CTLs within infected tissue allows efficient target localization. *The Journal of Immunology*, **195**(11), 5285–5295.

49. Rajakaruna, H., O'Connor, J. H., Cockburn, I. A. & Ganusov, V. V. 2022 Liver environment-imposed constraints diversify movement strategies of liver-localized CD8 T cells. *J Immunol*, **208**, 1292–1304. doi:10.4049/jimmunol.2100842.

50. Budhu, S., Loike, J. D., Pandolfi, A., Han, S., Catalano, G., Constantinescu, A., Clynes, R. & Silverstein, S. C. 2010 CD8+ T cell concentration determines their efficiency in killing cognate antigen-expressing syngeneic mammalian cells in vitro and in mouse tissues. *J Exp Med*, **207**(1), 223–35.

Mathematical modeling suggests that a single Plasmodium-specific CD8 T cell can eliminate a malaria liver stage in mice

Soumen Bera, Rogerio Amino, Ian A. Cockburn, and Vitaly V. Ganusov

Supplemental Information

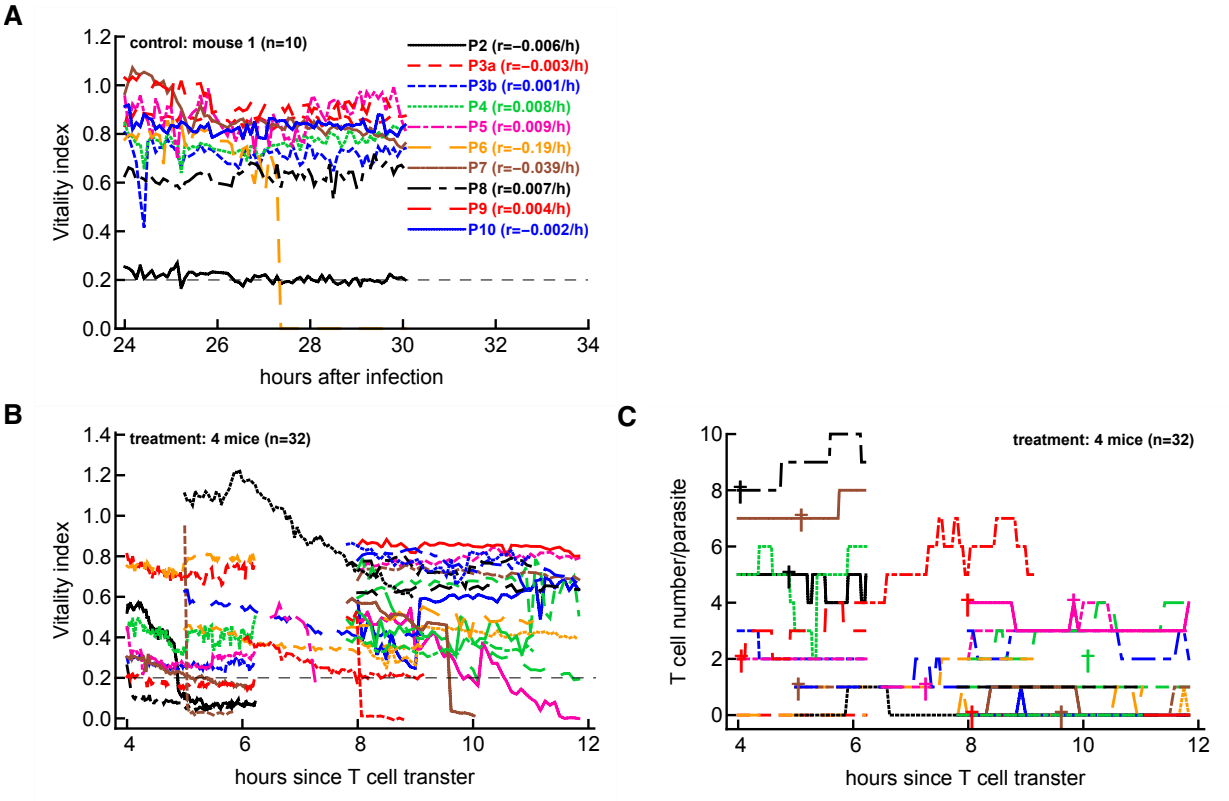

Supplemental Figure S1: Detailed data on dynamics of VI and T cell numbers in control and treatment groups of mice. (A) We plot the dynamics of parasite's VI for a subset of parasites ($n = 10$) in one of the two control mice along with estimated rates of VI change over time r. (B) We plot the dynamics of parasite's VI from 32 parasites in 4 mice in treatment group. (C) We plot the dynamics of T cell numbers located near each of the liver stages in B. Crosses indicate parasites that eventually died during the imaging (VI dropped below 0.2). In panel A&B dashed horizontal line denotes the threshold for a dead parasite (VI = 0.2). Note that in panel A time is in hours since infection and in panels B-C time is in hours since T cell transfer (that occurred 20 hours after the infection, see **Figure 1**A). Data for individual parasites are also shown in **Supplemental Figures S2 and S4**.

Model	β_1	β_2	β_3	β_4
	4-11 hours			
Log-logistic	0.9536	0	100	3.2
Weibull I	0.7	0	100	5.66
Weibull II	0.287	0	100	2.386
Lognormal	-0.6	0	100	3.2
Exponential decay	NA	4.99	0	100
	4-6 hours			
Log-logistic	0.47	0	100	0.74
Weibull I	0.29	0	100	2.39
Weibull II	-0.39	0	100	0.31
Lognormal	-0.29	0	100	0.73
Exponential decay	NA	2.92	0	100
	6-8 hours			
Log-logistic	0.92	0	100	2.02
Weibull I	0.61	0	100	3.89
Weibull II	-0.7	0	100	1.14
Lognormal	-0.57	0	100	2.03
Exponential decay	NA	3.27	0	100
	8-11 hours			
Log-logistic	15.77	0	100	143.89
Weibull I	276.2	0	100	7054.2
Weibull II	-2875.7	0	100	7088.4
Lognormal	-749.03	0	100	11301.5
Exponential decay	NA	18.85	0	100

Supplemental Table S1: Estimated parameters of the dose response models. We fitted log-logistics (eqn. (1)), Weibull I (eqn. (2)), Weibull II (eqn. (3)), lognormal (eqn. (4)), and exponential decay (eqn. (5)) models to normalized VI data divided into different time periods (4-8, 6-8, 8-11, and 4-11 hours post T cell transfer, see Materials and methods for more detail). Model fitting was done using `drc` package in R. Estimated parameters are β_1 (slope), β_2 (lower limit), β_3 (upper limit), and β_4 (ED50), and NA denotes not applicable. Values for lower and upper limits were restricted to 0 and 100, respectively.

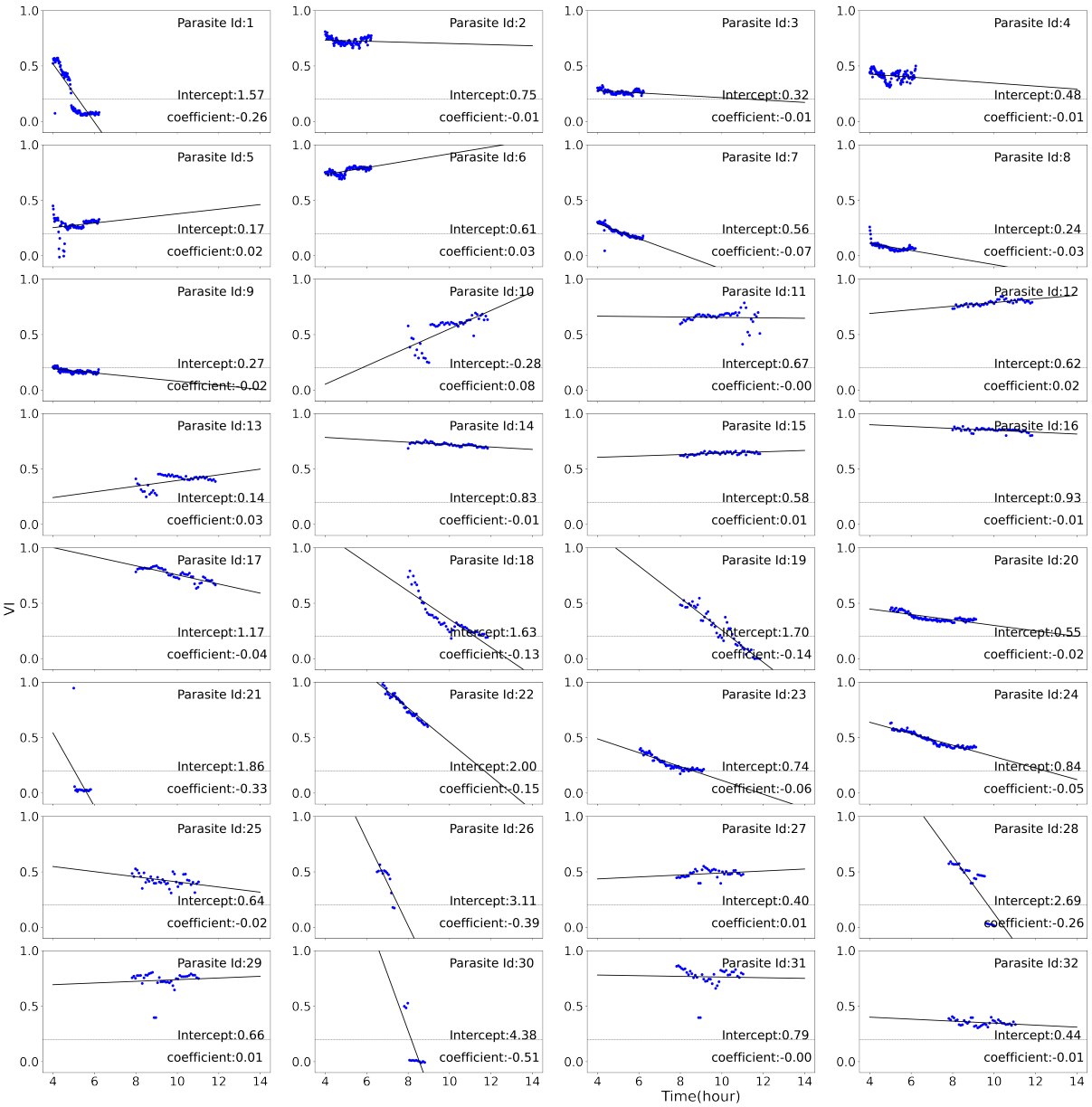

Supplemental Figure S2: Variable dynamics of the parasite's VI with time for all 32 parasites in the data. We performed linear regression of VI vs. time and parameters of the regression (slope and intercept) are indicated on individual panels. Regressions were performed using **scipy.stat** python package. Dotted horizontal line represent the VI = 0.2 cutoff for dead parasites.

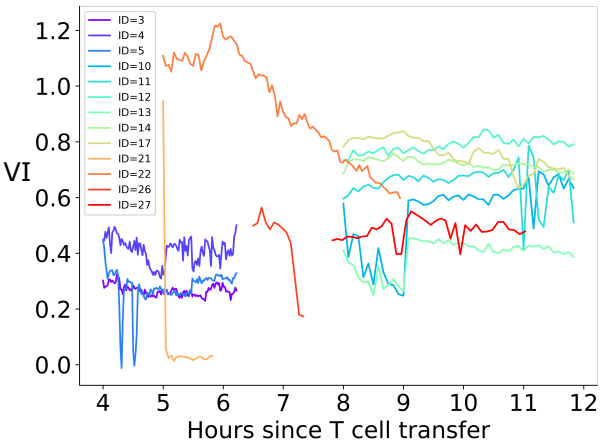

Supplemental Figure S3: Stability in parasite's VI dynamics with non zero T cells over time. We show the dynamics of VI of parasites that had some T cells nearby but did not die during the observation period (i.e., VI remained above 0.2). The correlation between VI and T cell numbers for these parasites is non-negative and thus, these were excluded from some of the analyses. The data are colored from violet to red based on the parasite ID number.

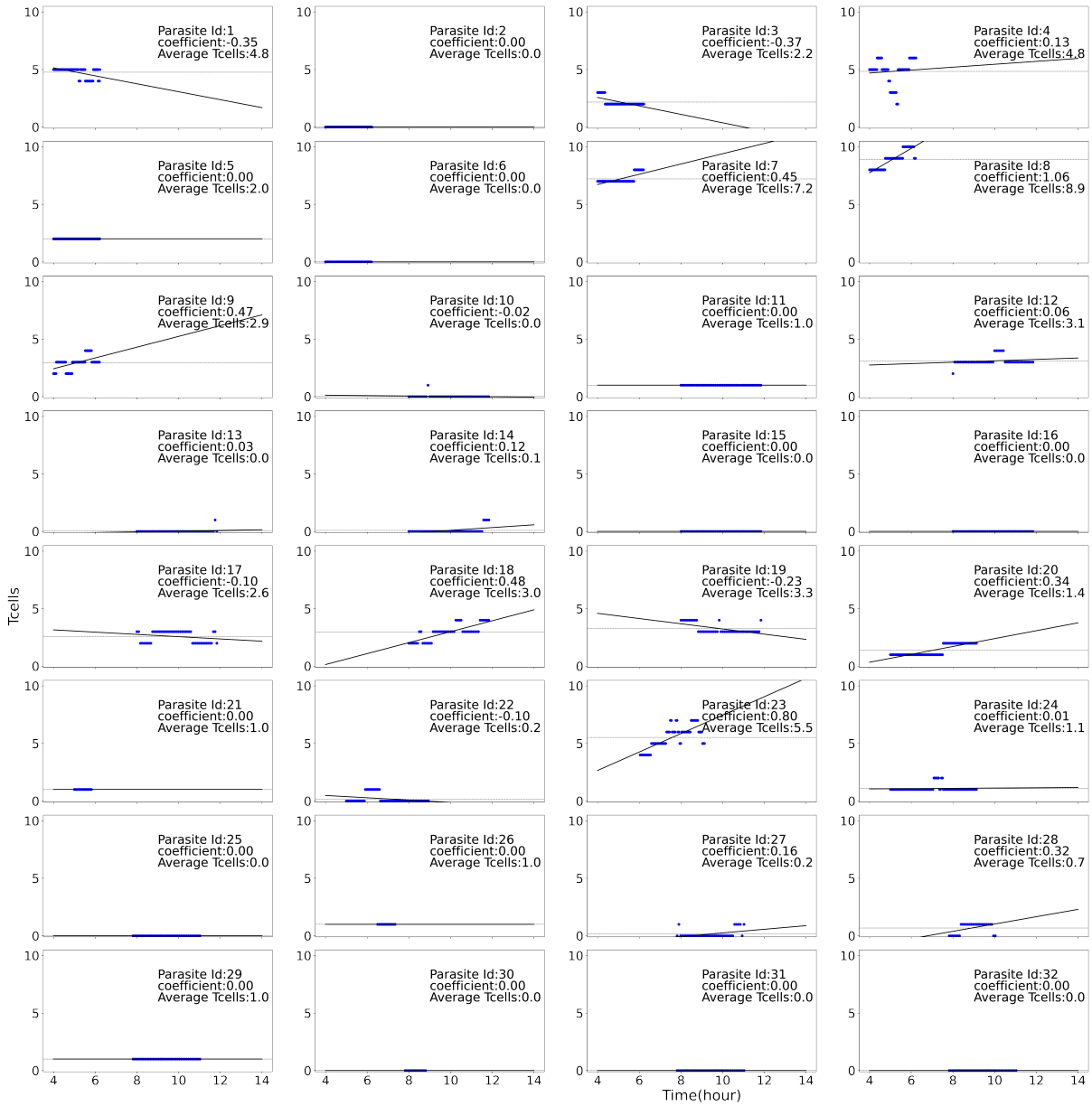

Supplemental Figure S4: Dynamics of T cells near each of 32 parasites. The slope (coefficient) and intercept of the T cell's trajectory was calculated using *scipy.stat* Python package. Dotted horizontal line represent the average number of CD8 T cells per parasite. Parasites with following IDs did not have any T cells nearby during the imaging period: 6, 15, 16, 25, 31, 32.

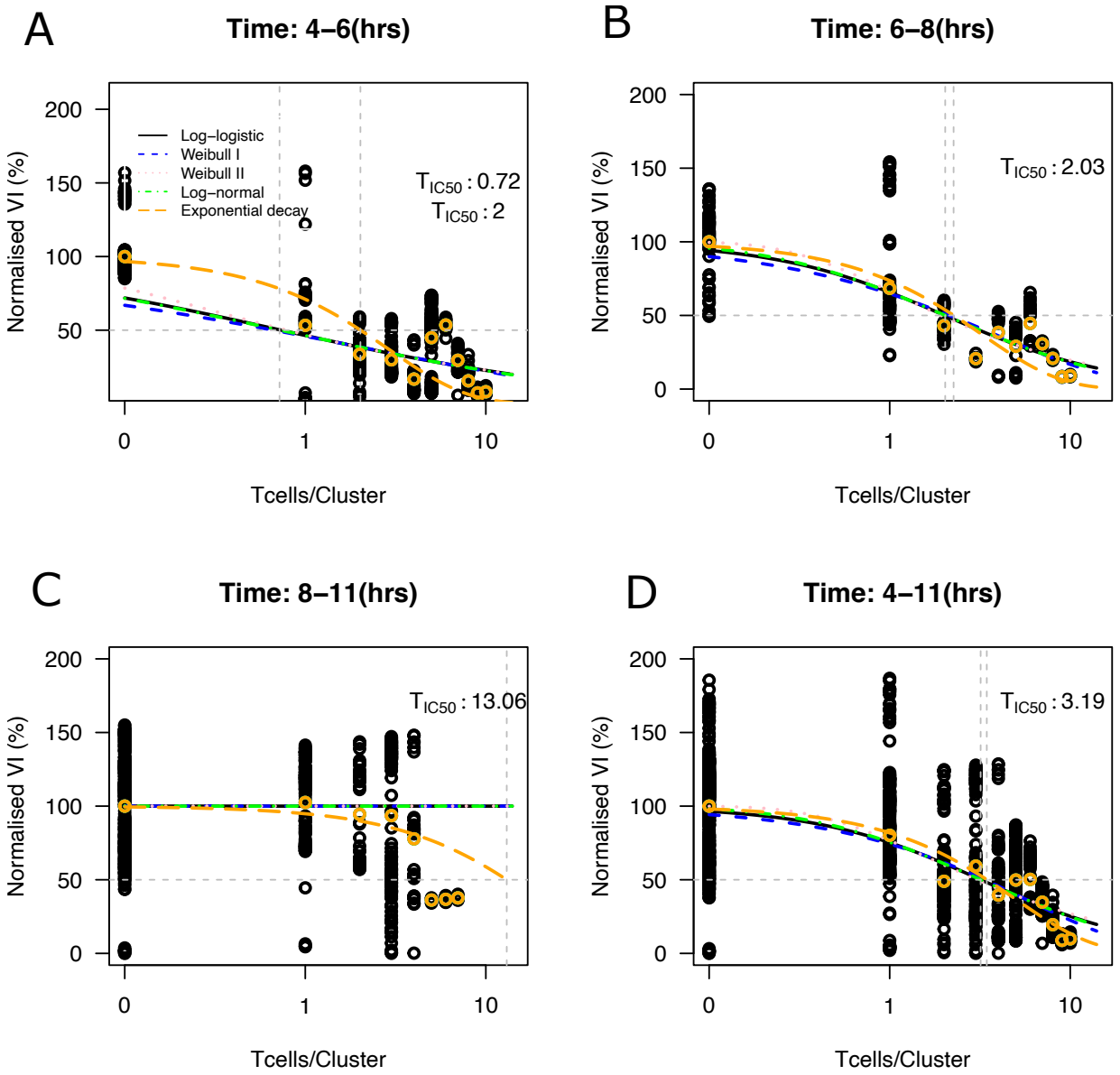

Supplemental Figure S5: Higher numbers of T cells per parasite are needed to reduce parasite's VI by 50% at later times since T cell transfer. We fitted several dose-response functions (eqns. (1)–(5)) to normalized experimental data on VI values for all time points with T cell numbers as a "dose". Data were normalized to their initial value. (A-C) Datasets were partitioned in different time periods (4-6, 6-8, and 8-11 hours after T cell transfer) (D) The models were fitted to all data. A decision-tree based approaches is used to select the best fit model among the candidates using AIC in R package *drc*. The predicted number of T cells at which VI reaches 50% of its initial value (T_{IC50}) is shown on individual panels by the dashed vertical lines. Dashed horizontal lines denote 50% of initial VI. Parameters of the best fit models are given in **Supplemental Table S1**.

Parasite ID	Null Model (no T cell)	Model (with experimental T cells)			Model (increasing T cell/15 mins)			Model (increasing T cell/30 mins)			Model (increasing T cell/60 mins)		
	P, 1/hr	**P, 1/hr**	α	**k, 1/hr**	**P, 1/hr**	α	**k, 1/hr**	**P, 1/hr**	α	**k, 1/hr**	**P, 1/hr**	α	**k, 1/hr**
1	-0.036	0.0877	1.555	0.0381	-0.011	9.332	1.178	0.2443	**1.4139*****	0.0728	0.9628	**1.132*****	0.2206
3	-0.0019	0.0105	9.069	177.7	0.0196	**12.07****	5876	0.0224	**9.616****	389.8	0.0369	**6.55***	15.22
4	-0.0015	0.0355	7.356	1.664	**0.0649***	**7.256****	1.829	**0.055***	**7.154***	1.633	0.06	6.136	0.888
5	-0.0149	-0.179	-0.073	-0.021	**-0.096****	**-0.358****	**-0.0025***	**-0.1167****	**-0.274***	**-0.005***	**-0.127****	-0.257	-0.008
7	-0.016	0.3475	**1.334*****	0.083	0.3224	**1.59*****	0.095	0.3628	**1.638*****	0.121	0.362	**1.6381*****	0.121
8	**-0.049*****	0.2662	**1.4627*****	**0.1055*****	0.2499	**1.548*****	**0.114*****	0.3052	**1.4583*****	**0.1149*****	**0.3052***	**1.4583*****	**0.1149*****
9	-0.0036	**0.0521****	4.152	4.63	**0.0828*****	**7.201*****	882.1	**0.078****	**5.529*****	66.15	**0.072***	**4.283*****	9.265
12	0.0013	0.008	21.14	0.2239	0.0073	27.64	0.26	0.007	29.04	0.556	0.007	28.22	0.7046
13	-0.005	-0.0051	2.25	0.0118	0.006	23.15	2.6e5	0.007	22.44	3.3e5	0.007	22.44	3.3e5
14	-9e-05	0.0012	**145.1*****	4.5e20	**0.0125****	**30.88*****	29.88	**0.0105***	**33.91*****	187.4	**0.0076***	**31.82****	182
17	-0.0035	0.0028	3.0855	0.0042	0.0279	**5.4811***	0.0138	**0.0421***	**6.1223*****	**0.0316***	0.0457	**4.7322*****	0.032
18	-0.0374	0.0419	**1.8391****	0.0586	**0.172***	**2.621*****	**0.1624****	0.0744	**2.4047*****	0.0989	**-0.0265***	63.93	150000
19	-0.0393	**-0.4337***	**0.7558*****	-0.0906	0.1968	**1.9948*****	**0.0868***	**0.3357***	**1.7309*****	**0.1374***	0.3447	**1.466*****	0.1309
20	-0.0031	0.0089	6.6652	2.1162	**0.0351****	**8.7531*****	13.704	**0.0259***	**9.1719*****	24.67	0.0202	**7.6859*****	7.643
22	**-0.0059***	-0.0045	10.14	0.0014	0.0074	**3.068****	**0.0032***	0.0058	**3.55****	**0.006***	0.0197	**2.717*****	**0.015****
23	-0.0126	**0.203***	**1.9964*****	**0.1476****	**0.3146*****	**2.5811*****	**0.353*****	**0.3365*****	**2.2805*****	**0.3202*****	0.1764	**1.8378*****	**0.1182***
24†	**-0.0055***	-0.0036	339.6	2.6E66	-0.0011	**28.34*****	1.6e4	0.0184	**7.6052*****	0.8049	**0.04****	**5.517*****	**0.5883*****
27	-0.0005	0.0023	7.2209	1.803	**0.037***	**13.97***	108.08	0.0304	**13.43***	153.32	0.0125	29.24	1.5e07
28	-0.0455	-0.0105	0.6655	0.0457	0.0309	3.3187	0.1683	0.0183	3.4518	0.3911	-0.0176	11.008	226.7

Supplemental Table S2: Estimated parameters of the forecasting model in which the number of T cells per parasite was assumed to increase over time at different time intervals. The null model (without T cell, eqn. (14)), or forecasting model with experimentally measured T cell numbers or when we assumed a steady increase in T cell numbers per parasite (eqn. (15)) were fitted to data. All the forecasting models were compared with the null model using ANOVA. Model fitting was done by R package *minpack.lm*. Statistical significance code shown with bold where '***p'< 0.001, '**p' < 0.01, and '*p' < 0.05. † represent model fitted with data without convergence.

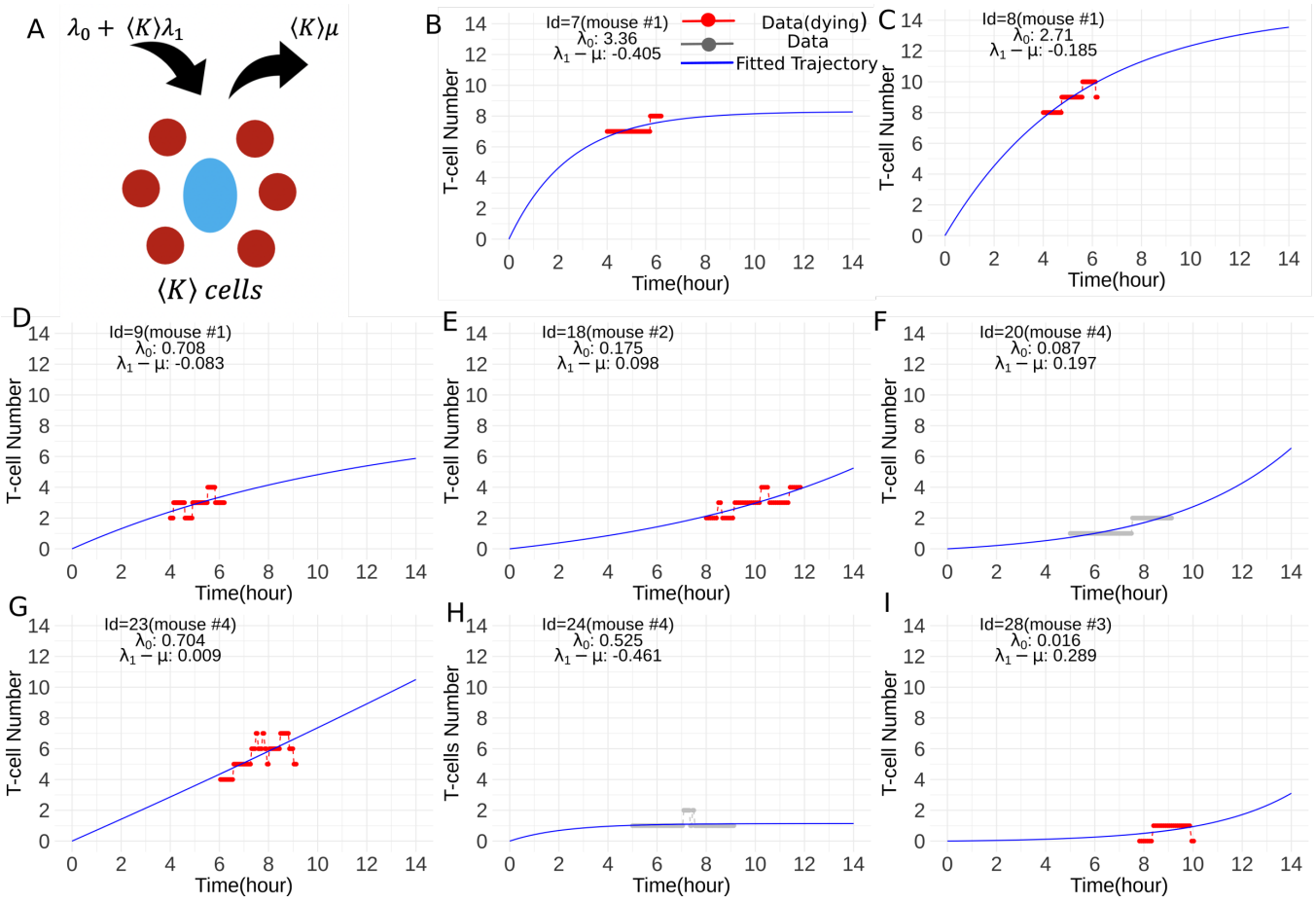

Supplemental Figure S6: Density-dependent recruitment model describes well the change in the number of T cells different parasites. (A) Schematic of the mathematical model of T cells cluster formation around Plasmodium yoelii (Py)-infected hepatocyte in mice. The rate of T cell entry in the cluster is $\lambda_k = \lambda_0 + k\lambda_1$ and exit from the cluster is μ_k, where k is the number of T cells near the parasite. (B-I) We fitted the DDR model to the data on change in T cell number over time for several parasites for which there was a negative correlation between VI and T cell numbers. The color of the data (red or gray) denote dying or not dying parasites (based on their VI dynamics). Fitting was done using `nls` routine in R using nonlinear least squares.

Parasite ID	VI(0)	Average T cell number	Killing rate k, 1/h
7	0.2994(±0.007)	7.2	0.0454(±0.132)
8	0.1238(±0.007)	8.9	0.0586(±0.158)
9	0.1909(±0.003)	2.9	0.0374(±0.085)
18	0.6747(±0.033)	2.9	0.1437(±0.120)
20	0.4136(±0.007)	1.4	0.0463(±0.032)
23	0.3694(±0.008)	5.5	0.0457(±0.039)
24	0.5939(±0.006)	1.1	0.1012(±0.278)
28	0.517(±0.055)	0.68	5.7825(±1.601)

Supplemental Table S3: Parameter estimates of the simple mathematical model and their standard error. We fix this parameter after fitting model with each parasite data corresponding CD8 T cell response and estimate per parasite killing efficacy per hour. Here, growth rate of the parasite r is close to zero which perfectly matches estimates found in control experimental data. Parasite ID is chosen those following negative correlation with T cell number out of 32 parasites. Standard errors for the parameter estimates were provided by the *lmfit* function of the scipy package in python. The average killing rate for 7 parasites (excluding ID=28) $\bar{k} = 0.068$/h.

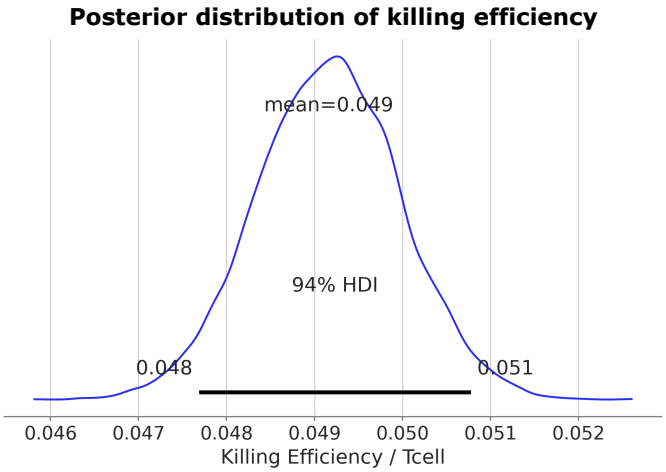

Supplemental Figure S7: Killing efficiency by CD8 T cells estimated using Bayesian approach. We fitted the mass action killing model (eqn. (17)) to the data on the dynamics of VI for 8 parasites that showed negative correlation between VI and T cell numbers (**Figure 4**B-I) using a Bayesian approach (see Materials and methods for detail). Posterior distribution (no u-turn sampling to produce 10000 posterior samples from 2 independent MCMC chains and uncertainty with a thick-tailed half Cauchy prior for the killing efficiency k. For fitting we used *PyMC3* package in python. Killing rate k is in per hour units.

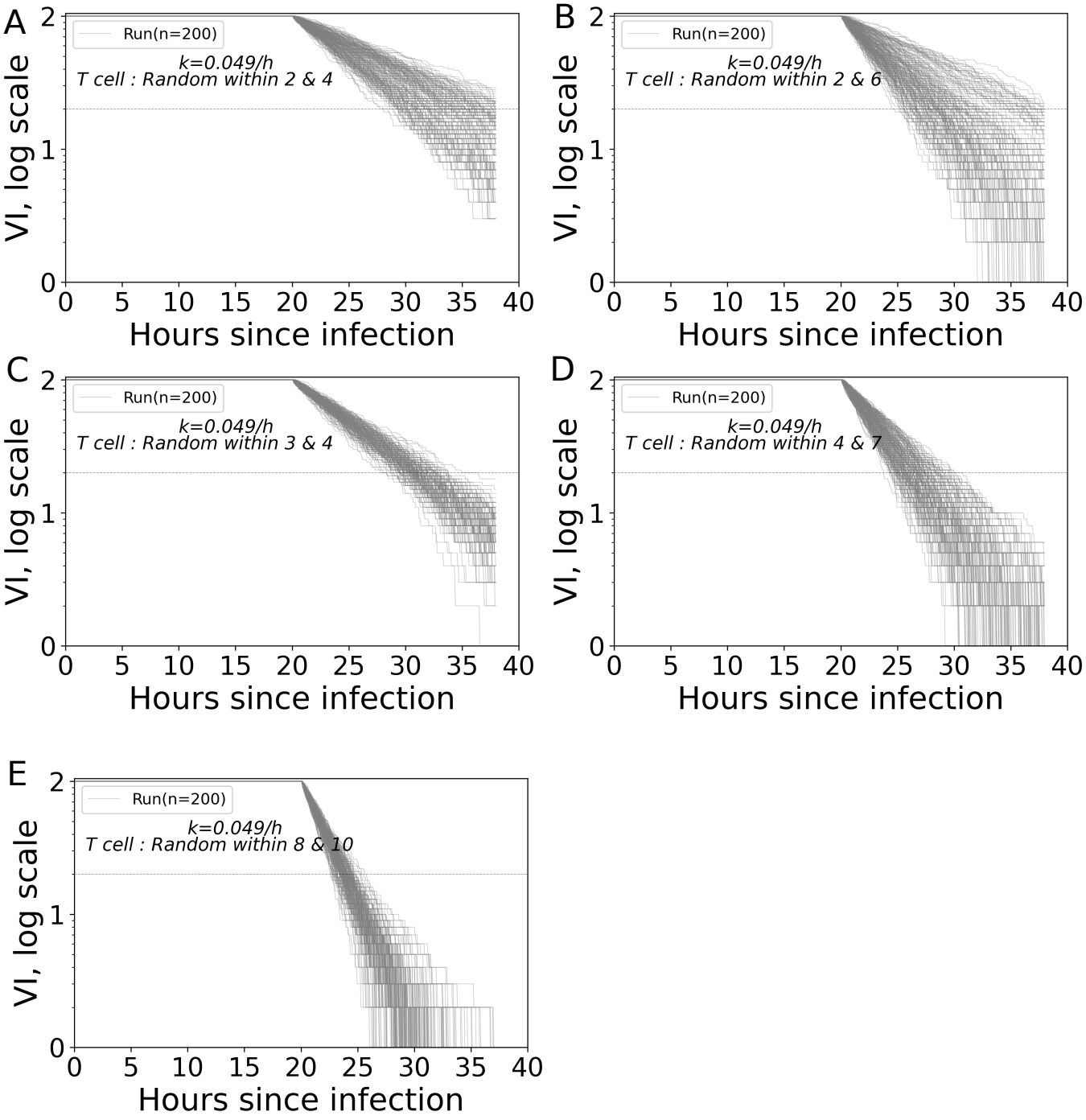

Supplemental Figure S8: Stochastic simulations of VI dynamics are inconsistent with constant VI observed for most parasites. We performed stochastic simulations of VI dynamics assuming the model with mass-action killing ($k = 0.049$/h) using Gillespie algorithm. To mimic our experimental design we simulated the model for 20 hours without any CD8 T cell with a minimal parasite's growth rate. Then we adding a random number of T cells (chosen 200 times from a uniform distribution with limits indicated on individual panels and taken from the actual range observed for individual parasites) and simulated the dynamics for the next 16 hours. Dotted line shown the VI threshold of a death parasite. The simulations were done using Python package *gillespy2* with *TauHybrid Solver* routine.

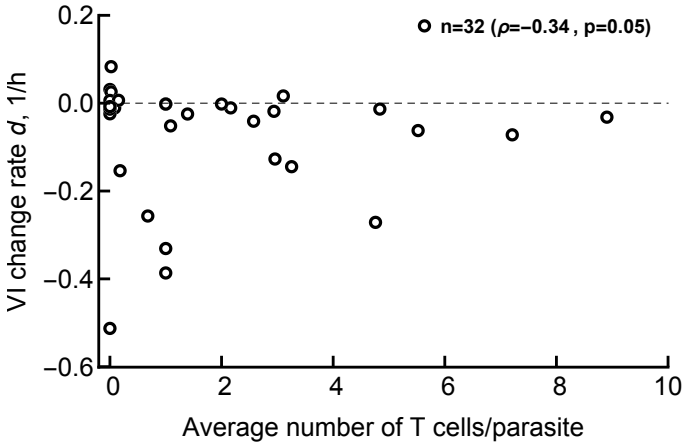

Supplemental Figure S9: The number of T cells per parasite is a relatively poor predictor of the VI change rate. For every of 32 parasites in our datasets we calculated the rate d of VI change with time using linear regression (see **Supplemental Figure S2**) and for the same parasites we calculated the average number of T cells observed in imaging experiments. Negative values for the change rate imply declining VI. Note that many parasites had only few T cells in their vicinity. Spearman rank correlation coefficient ρ and p value from the test is shown.